Publ. Astron. Soc. Japan **39**, 1–45 (1987)

Impact of X-Ray Observations from the Hinotori Satellite on Solar Flare Research*

Katsuo TANAKA

Tokyo Astronomical Observatory, University of Tokyo, Mitaka, Tokyo 181

(Received 1986 June 11; accepted 1986 October 8)

Abstract

The X-ray observations of solar flares from the Hinotori satellite are extensively discussed. Complex flare variety in the X-ray time profile, spectrum, and morphology is elucidated by considering three flare types (A, B, and C) and also five emission components. Various X-ray morphology and evolutionary characteristics are discussed in comparison with optical data. The type B (impulsive) flare is suggested to occur in complexly sheared low-lying fields after their separation from the erupted filament, followed by progressive energy releases at higher loop arcades in the gradual phase. The type C (gradual-hard) flare shows long-enduring energy releases at high loops with weak shear. Spectral hardening is shown to proceed with systematic shifts of the hard X-ray source to higher altitudes. The soft X-ray diagnostics of the hot flare plasmas are extensively discussed covering flare temperature diagnosis by Fe XXVI, Fe XXV, and continuum spectra, early development and the relation of nonthermal line broadening and blueshift, Kα diagnosis, and line polarization. The hot thermal source ($T_e > 3\times10^7$ K) emitting Fe XXVI and hard X-rays (<40 keV) is identified with the loops of high density and high field strength, originally confined at one leg of the erupted prominence, and shows sequential formation at higher altitudes. Suppression of acceleration in type A flares is suggested. A hybrid origin of the hot plasmas is implied from evidence for both evaporative supply and coronal in-situ heating. A large coronal energy deposit due to in-situ heating and dissipation of low-energy electrons is argued to support the conduction-driven evaporation. Observed flare variety is suggested to result from the diversity of intrinsic magnetic shear and ambient density in different magnetic-tube configurations that originate in the convection zone. A magnetic morphology of flares is suggested together with a general flare scenario.

Key words: Hard X-rays; Hinotori; Hot plasmas; Magnetic fields; Soft X-rays; Solar flares.

* The first in a series of invited review articles appearing from time to time in these publications.

1. Introduction

Research on solar flares has advanced greatly due to recent observations from space and from the ground. This review discusses comprehensively the results of X-ray observations from the Hinotori satellite, the first Japanese space mission devoted to solar flare observations. During the last solar maximum the first X-ray images in the hard X-ray (henceforth HXR) bands above 20 keV have been provided by the Solar Maximum Mission (SMM) and Hinotori. Detailed spectroscopic diagnostics of the hot flare plasmas has resulted following observations of emission lines from highly ionized metal ions from P78–1, SMM, Hinotori, and Tansei IV. Comprehensive continuum observations covering a wide energy range from the soft X-ray (henceforth SXR) to the gamma-ray with high time and spectral resolutions have been achieved by SMM and Hinotori. These observations, along with those from other spacecraft (ISEE-3 and PVO; Kane et al. 1979) and a balloon (Lin et al. 1981), have yielded the following major findings on the high-energy aspect of the flare:

(1) high energy (>150 keV) HXR is emitted from low heights (<2500 km),

(2) HXR sources are concentrated at footpoints of the coronal magnetic loops at the initial phase of the impulsive flare,

(3) extended and stationary HXR sources occur high up in the corona (>40000 km),

(4) an abundant superhot plasma component of $T>3\times10^7$ K contributes HXR continuum and Fe XXVI lines,

(5) large nonthermal random motions and upflows are seen in the high-temperature plasmas of $T>10^7$ K during the early flare phase,

(6) very prompt acceleration of electrons occurs over a wide range from deka-keV to deka-MeV together with concurrent accelerations of high-energy protons and ions in the impulsive flare,

(7) a strong anisotropy is observed for the gamma-ray radiation in $E>10$ MeV,

(8) microflares occur frequently in nonflaring active regions,

(9) flare X-ray emission showing a wide variety can be described with three classifications: A, B, and C.

These findings have provided a realistic image on timing, production site, and energy transport of high-energy particles. Some evidence is given for the model of thick-target nonthermal particle beams, but in general, HXR behavior is revealed, as stressed by the Hinotori observations, to be more complex showing cases of high-energy electrons trapped in the coronal loops and of thermal HXR emissions from the newly discovered hot thermal plasma component. In fact, discoveries chiefly by Hinotori of long-lived HXR sources in the corona and the compact hot thermal source producing strong thermal HXR emission and Fe XXVI lines have had a significant impact on flare research. The combined SXR and HXR observations have revealed various thermal and dynamical processes in a flaring loop such as "evaporation." The heating process, however, seems not to be explainable by a single process like evaporation. Hinotori contributed significantly to all the above findings except (1), (7), and (8) and clarified these complicated situations.

The solar flare is a complex dynamic phenomenon of rich variety. It starts with

a sudden release of the excess energy stored in the magnetic fields, and gives rise to impulsive acceleration, fast heating, and violent bulk motions, which may be the basic outputs observed commonly in the cosmic burst phenomena. The complexity of flares comes from simultaneous and multiple occurences of numerous MHD and resistive instabilities and subsequent energy transfers in a complex ensemble of magnetic fields. The flare energy is thought to be stored in a particular configuration represented as a magnetic shear. The active regions show various magnetic morphology with different degree and extension of the magnetic shear. Energy releases taking place in these intrinsically diverging magnetic configurations would inevitably result in a wide variety of their patterns and developments. Hinotori has provided an important step to understanding of the wide range of X-ray behavior by permitting systematic flare grouping based on X-ray morphology, spectrum, and time profile (9). It has also clarified basic environmental conditions that lead to flare variety. These aspects are emphasized in this review.

Hinotori was a compact (190 kg) spinning satellite produced and launched by the Institute of Space and Astronautical Science (Y. Tanaka 1983). Unique techniques were adopted to use the satellite rotation for acquiring X-ray images (Oda 1965) and for obtaining X-ray line spectra (Tanaka and Nishi 1978; Tanaka 1986b). The five instruments aboard Hinotori were (1) rotational modulation collimators for X-ray imaging in the two bands of 15–40 keV (25–35 keV in some cases) and 6–13 keV, (2) two rotational Bragg spectrometers for Fe line (Fe II–Fe XXVI) spectroscopy in the region of 1.73–1.95 Å, (3) a gas scintillation proportional counter for the detailed continuum spectrum in a region of 1.5–17 keV (12 keV in some cases), (4) a scintillation detector for the hard X-ray spectrum from 17 keV to 300 keV, and (5) a scintillation detector for the gamma-ray spectrum from 300 keV to 6.7 MeV. A description of these instruments has been given by Kondo (1982). All the instruments operated successfully throughout the entire period from 1981 February 26 through 1982 October 8 and, by viewing the full sun, obtained an enormous amount of data from 720 flares in total. Thus X-ray images and spectra could be obtained from a number of large flares including 31 X-class flares, which enabled a comparative study of many types of flares. Previous reviews of the Hinotori results have been given by K. Tanaka (1983), Takakura (1985), Tsuneta (1984a), Watanabe (1984a), Takakura et al. (1984c; henceforth TTH84), Nishi and Tanaka (1984), and Tanaka (1986a). Some results from Hinotori were discussed in the SMM Workshop (Kundu and Woodgate 1986). The present review includes more recent results, especially on comparative studies with the optical observations.

2. Flare Variety in the X-Ray Emissions

The HXR radiation shows that energetic electrons are produced in flares. They may be stopped instantaneously at the dense layer emitting HXR photons in a "thick target" scenario or they may be trapped in (or escape from) a magnetic loop emitting "thin target" X-rays. The energetic electrons may be called "nonthermal" if their energies exceed substantially the energy of the ambient plasma, but called "thermal" if the bulk of the plasma itself has a high enough temperature to produce HXR. The

HXR burst marks the onset of a flare and generally continues for a relatively short duration showing rapid variations. The flare also produces an SXR emission, which shows a monotonic, smooth increase in contrast to the HXR burst and peaks after the burst. This manifests the production of an abundant thermal population with $T_e > 10^7$ K. The actual HXR burst profiles exhibit a remarkable variety from flare to flare. The majority of the bursts present an impulsive time behavior characterized by rapidly varying spikelike emissions coincident over a wide energy range (figures 1a and 1b). In some flares the impulsive variation changes in the course of the flare to a smoother, gradual time variation (figure 1c). A smaller number of flares show gradual time variation throughout the entire flare period. Two types of gradual variation can be identified: one with a very soft spectrum (figure 1d) and the other with a very hard spectrum (figure 1e). The low-energy flux (<40 keV) of the former show a time profile very similar to that of Fe XXVI Lα and has been demonstrated as the thermal emission from newly discovered hot thermal plasma of $T > 3\times10^7$ K which is responsible for the Fe XXVI lines. The latter is further characterized by broad emission peak(s) and systematic spectral hardening that leads sometimes to a delay of the peak towards the γ-rays in strong contrast with the impulsive type.

In assessing the new HXR images made by the SMM and Hinotori, it is of considerable interest to establish whether or not the HXR sources have a strong concentration at the footpoints of the magnetic loops as predicted by the "thick-target nonthermal" electron beam model (cf. Emslie 1981). High brightness at the footpoints is also predicted in the "thermal" model of the impulsive burst as expanding thermal fronts reach the footpoints immediately (Smith and Auer 1980). Prior to the hard X-ray imaging stereoscopic observations using two spacecraft, PVO and ISEE-3, had provided evidence for low source altitude ($h<2500$ km) for $E=150$ keV X-rays (Kane et al. 1979). Early results from the SMM HXIS emphasized concentration of the HXR emission at 16–30 keV at the two footpoint in the impulsive phase (Hoyng et al. 1981; Machado et al. 1982). The results from the Hinotori SXT, on the other hand, showed that the HXR images made at an effective energy of 25 keV are mostly single; either compact or extended. According to TTH84, 22 of 30 flares show single sources. The source extends to the whole coronal loop and possibly includes the footpoints, but the peak brightness is located mostly in the loop region. Strong evidence is also given for persistent emission from above the limb in some gradual flares. It has been revealed also that many of the HXIS results show single, unresolved sources (Duijveman and Hoyng 1983).

The Hinotori researchers discussed these complex phenomena by grouping flares with combined properties of the time profile, spectrum, and morphology. Ohki et al. (1983) classified impulsive and gradual types of flare. Types A, B, and C have been introduced by K. Tanaka (1983) and discussed by Tsuneta (1984b), Tanaka et al. (1983), Sakurai (1985), and Dennis (1985). Takakura (1985) used terminology *gradual soft*, *impulsive*, and *gradual hard* for these types. The three types have the following properties:

Type A (Hot Thermal Flare): the hot thermal plasma component of $T=3$–4×10^7 K is very effectively produced and emits the HXR for $E<40$ keV and strong Fe XXVI lines. The time profile shows a gradual rise and fall similar to the SXR

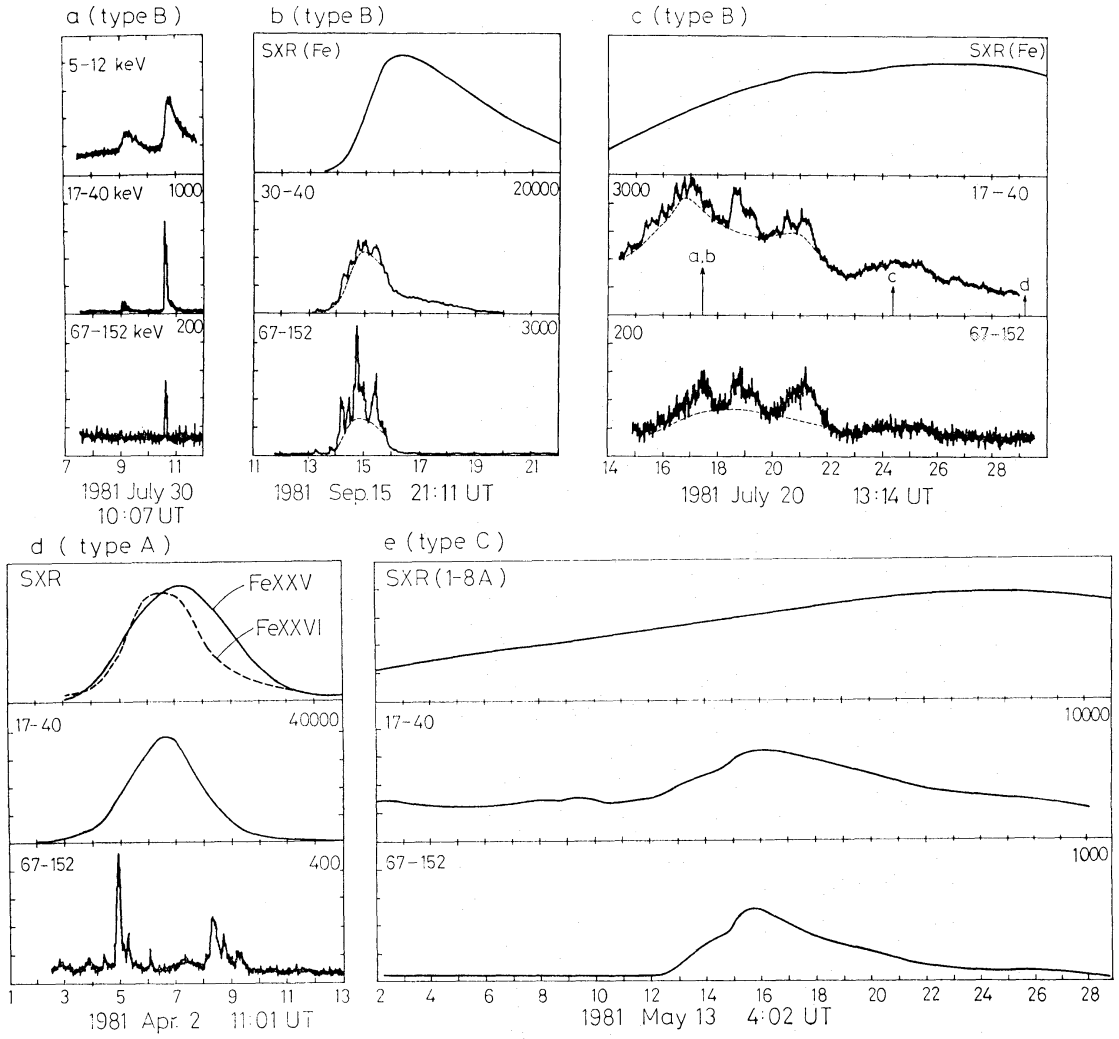

Fig. 1. Various flare time profiles in SXR (top section) and two HXR channels (middle and bottom sections) observed from Hinotori. The same time scale is used for all (one division corresponds to 1 min). SXR (Fe) represents total count in the Fe-line complex at 1.7–2Å and SXR (1–8Å) denotes the flux in 1–8 Å from GOES.

profile and the HXR source is compact (<5000 km). The HXR spectrum above 40 keV is soft (effective power-law index $\gamma=8$–9). Radio emission is weak.

Type B (Impulsive Flare): typical impulsive HXR burst consisting of rapidly varying spikes, emitted from the extended low corona including the footpoints. $\gamma=$ 3–7. Later phase of some flares evolves to a more gradual time profile with softer spectrum ($\gamma=5$–8) and to a more compact source structure located at higher altitude.

Type C (Gradual-Hard Flare): a long-enduring (>30 min) burst with broad peak(s) showing no impulsive variation. The source is located high up in the corona ($h>40000$ km) and identified with large extended loops. The spectrum is very hard, well characterized by a power law ($\gamma=2.5$–4) and shows a systematic hardening with time. Microwave emission is very strong.

Type A seems to produce very effective heating but inefficient acceleration despite its high magnetic fields (300 G), whilst type C appears to be a very efficient accelerator despite its relatively weak fields (50 G). Also the time scale of the acceleration seems

1987PASJ...39....1T

Table 1. Five X-ray emission components.

Component	Time profile and spectrum	X-ray morphology	Hα morphology	Suggested origin	Type of flare
I. Impulsive component	Impulsive variability (spikes) Power law or exponential $E>15$ keV (some $E>5$ keV; type A $E>40$ keV)	Footpoints + low corona (source shrinks and shifts later)	High magnetic shear Filament eruption Irregular spread along inversion line→two-ribbon spread	Impulsive accelerations (energization) in complexly sheared fields (immediate decay)	Impulsive phase of type B
II. Gradual-hard component	Spikeless broad peak(s) Power law (hard spectrum) Spectral hardening beyond peak(s)	Extended at high corona (2–9×10^4 km) Stationary or shift to higher altitudes	Large-scale weak-sheared configuration Filamentless region Two-ribbon spread at distance	Progressive accelerations across large-scale fields (partial trapping)	Type C Gradual phase of type B
III. Hot thermal (superhot) component	Gradual rise and fall T_e: 3–4×10^7 K (Fe XXVI diagnosis) HXR excess emission at 10–40 keV (thermal)	Compact loops (progressive shift to higher altitudes) High $n_e(\geq10^{11}$ cm$^{-3})$	Bright loops appear with short delay Two-ribbon spread (kernel)	In-situ coronal heating Complementary to impulsive component	Type A Gradual and peak phases of type B
IV. SXT thermal component	Flux $\propto\int^t$ (impulsive component) dt (type B) Gradual rise uncorrelated with impulsive component (type C) Upflows and nonthermal random motions (initially) $T_e\geq10^7$ K	Diffuse extended emissions with peaks at footpoints →loops	Two-ribbon (extended) loops at later stages	Evaporation+in-situ coronal heating	All flares
V. Quasi-thermal component	Gradual variation Background enhancements 20–70 kev	Extended at corona	Two ribbon (diffuse)	Nonthermal or thermal ($>5\times10^7$ K)	Gradual phase of type B Background of types B and C

to be quite different between type B and type C suggesting different modes of acceleration and emission mechanisms. On the other hand, these types, on circulated as a "flare classification" (in the SMM Workshop: Kundu and Woodgate 1986), have brought about some controversy. Some flares have been shown to have characteristics of both types B and C (de Jager and Švestka 1985). Actually the later phase of the type B flare often shows characteristics of type A or type C. It should be emphasized that the three types have been introduced to clarify some distinctive properties appearing in particular flares, and are not intended as a flare classification in the strict sense such as was done for the Skylab flares by Pallavicini et al. (1977). K. Tanaka (1983), in fact, used also the terminology of type A, B, and C "phases."

The spectral and temporal properties of X-ray radiation in the energy region 5–40 keV, where thep resent X-ray images were obtained, are highly diverse. It has been proposed (TTH84) that this diversity may be understood by introducing five emission components: (1) *impulsive*, (2) *gradual-hard*, (3) *SXR thermal*, (4) *hot thermal*, and (5) *quasi-thermal* (table 1). Actuaı flares are considered to comprise various combinations of these components. These emission components refer also to associated plasma or particle components. The *impulsive component*, which characterizes the impulsive phase of the type B flare, normally appears above 15–25 keV and the energy region below 15 keV is dominated by the *SXR thermal component* which comes from $10–25\times10^{6}$ K plasmas produced in all flares. In some flares the impulsive component with a power-law spectrum can be traced to 7 keV (figure 7c; Tanaka et al. 1984). Numerous tiny flares show only the SXR thermal component with no impulsive component above 15 keV. The latter may be missing through being below the detector sensitivity threshold or may actually be absent. Among these flares are found some, which show more impulsive time behavior (rapid rise and decay) in the range of 5–10 keV than in the range below 5 keV (Watanabe et al. 1983). This suggests that the *impulsive component* may possibly extend to the 5-keV region (cf. Kahler and Kreplin 1971). There have been extensive arguments as to whether the impulsive component is of thermal origin due to the bulk energization to $T>10^{8-9}$ K or of nonthermal origin due to the growth of tail in the Maxwellian distribution. The spectral distribution of about two hundred flares studied by N. Nitta (private communication; cf. Nitta et al. 1983) reveals that the exponential fit is better in the rising phase of some 70% of type B flares than the power-law fit, while the power-law fit becomes better after the maximum phase. It is also found that the rising and falling phases of individual spikes tend to be fitted better by the exponential and the power law, respectively. Type C is fitted better by the power law. The exponential spectrum does not necessarily indicate the "thermal" model as in the case of composite spectra from multiple sources of different power-law spectra. It may simply manifest an enhanced emission around 60–100 keV region due to an excess population of the electrons at this energy. Conversely a power-law spectrum is realized in the "thermal" model due to a superposition of multi-temperature distribution (Smith and Auer 1980). Yoshimori et al. (1985) have shown that combined HXR and γ-ray spectra (20 keV–7 MeV) show a hardening above 300 keV clearly deviating from a single power-law or exponential spectrum below it (figure 7d). A different population of electrons may be inferred in higher energies or it may be due to contribution from unresolved nuclear lines. While the

"nonthermal" versus "thermal" arguments remain unresolved, the HXR emission that can be judged definitely of thermal origin has been designated as the *hot thermal component* ($T=3$–4×10^7 K). This component shows a distinct excess in the low-energy region (15–40 keV) above the power-law or exponential spectrum which prevails in the higher energy. It appears in about half of large impulsive flares, preferentially, in the post-maximum phase. Type A represents a rare case exhibiting this component throughout the entire flare period due to the absence of the impulsive component in the low energy. The *gradual-hard component* represents the HXR characteristics in the type C flares, though there are many intermediate cases which cannot be separated clearly from the impulsive component. The *quasi-thermal component* refers to the X-ray emissions that cannot be described by the above four components. For example, extended interval between the peaks in the type C flares (figure 6b) and some gradual phases of the type B flares (figure 1c) are characterized by an enhanced emission at 20–70 keV with the absence of the Fe XXVI emission which indicates the hot thermal component. Its temporal behavior is rather similar to the SXR thermal component. Either thermal origin from $T>5\times10^7$ K or nonthermal origin may be suspected. It may be pointed out that even the impulsive component may be contaminated by the quasi-thermal or hot thermal components. The impulsive spike component is often superimposed in a gradually varying envelope or a background emission which is only pronounced at 20–70 keV (figures 1b and 1c, dotted lines). The contrast of the spikes to the background increases at higher energies. The relative significance of the spike to the background varies among flares and may define an impulsiveness of the flare. However, it is totally unknown whether this component consists of numerous unresolved spikes or manifests a real gradual component. With these complexity in mind we will now discuss detailed properties of various flares.

3. Impulsive Flares (Type B)

The principal characteristic of the impulsive flare is its impulsive variability. A simple elementary impulsive burst may consist of one or two spikes as illustrated in figure 1a. The main spike has a FWHM of 5s and is accompanied by SXR emission (the SXR thermal component) which increases by precisely tracing the time integral of the HXR profile and has a longer duration of FWHM 20 s (Tanaka et al. 1982c). In general impulsive flares show a chain of spikes of random amplitude for a duration from tens of seconds to 10 to 20 min with or without an accompanying "gradual phase." This phase shows a smooth, spikeless time profile and may be contributed by either of the hot thermal, quasi-thermal or gradual-hard components. The peaks of the spikes show remarkable coincidence over a wide energy range from deka-keV to deka-MeV including the γ-line emission within the detector resolution of about 1 s (Kane et al. 1986). This high synchronism generally implies prompt simultaneous accelerations of electrons and ions. However, some exceptional cases are reported such as a γ-ray peak preceding by about 10 s HXR peaks (Yoshimori et al. 1986) and a systematic delay (about 5 s) of the γ-ray peaks to the HXR peaks in a periodically (8 s) pulsating event (Nakajima et al. 1983). The latter may imply two-step accelera-

tions but seems unusual. Subsecond variations reported by Takakura et al. (1983a) and variations on the order of tens of millisecond reported by Kiplinger et al. (1983) may give a constraint on the shortest acceleration time. The SXR thermal component shows an increase roughly proportional to the time integral of the HXR impulsive component. In the SXR lines, large line broadening (150–250 km s^{-1}) and blue-shifted subcomponent (300–400 km s^{-1}) are usually associated in the early phase of this type of flares (subsection 5.1).

A key question in the HXR images of the impulsive burst may be whether or not individual spikes come from different portions as would be expected in the elementary flare burst hypothesis (cf. de Jager 1979). The shortest flares that enabled imaging by the rotational modulation collimator with the time resolution of about 10 s have a duration of 20–30 s and consist of a few spikes (Takakura et al. 1983b). The HXR source contours are roundish with the FWHM of about 10″. Although this size is less than the nominal instrumental resolution (30″), structures as small as 10″ could be synthesized reliably with techniques like the maximum entropy method (cf. Tsuneta 1984a) as the collimators had a very sharp fringe pattern (Makishima 1982). In successive 10-s intervals changes of fine structures in the contour map and/or shift of the contour centroid of about 10″ occur, suggesting that the individual spikes are emitted from slightly different portions. In longer duration bursts sequences of the images made every 10 s often show jitterlike fluctuations in the peak position or more obviously in the contour shapes of low-intensity levels. But the whole source structure remains remarkably stable in the time scale of individual spikes except for a few cases (cf. Kosugi and Tsuneta 1983). On the other hand, a systematic evolution with much longer time scales is generally found. As given in a typical example by Takakura et al. (1984a; figure 2), the source is large and elongated in one direction (85″×40″ at 10% level of the peak in the contour) during the initial phase of rising flux, and then shrinks and becomes more roundish (30″×30″). This transition occurs rather abruptly around the burst peak during a continued spiky time profile. Furthermore a systematic shift of the source centroid, possibly to higher altitudes, occurs with apparent velocity of 20–40 km s^{-1}. Comparison with the two well-defined Hα ribbons reveals an accord of source elongation in the early phase with the inversion line of the longitudinal magnetic fields. In addition the HXR source fills the entire region between the two ribbons including the Hα ribbons, i.e., the footpoints of the magnetic loops. The smaller sources in the post-maximum are obviously isolated from the footpoints and located in the corona.

The extended and rather stable HXR source structure in the early phase seems to result from unresolved multiple emissions from low-lying elongated magnetic features connecting scattered footpoints with different orientations and lengths. This may be well illustrated in a very large X12-class flare of 1982 June 6 studied by Tanaka and Zirin (1985; henceforth TZ85). Evolution of the He I D3 emissions representing footpoint kernels, as reproduced in figure 2b, indicates that fast flashes spread along the whole inversion line in the initial phase, and later two ribbons develop and separate progressively, although restricted to a more local portion of the inversion line. The initial HXR source (figure 2c) extends over the region covering several isolated D3 footpoints which appeared simultaneously, and its contour peak agrees with one of

the optical kernels. At some other instants weak subpeaks appeared at different optical kernels. But, in general, the contrast and concentration of these peaks are low and most emission comes from extended space. Towards the later phase the HXR source shrinks to a more concentrated space between the two ribbons and the contours agree with those of the SXR peaks and the post-flare loops in D3 and Hα (figures 2e and 2f). One could safely conclude that the post-maximum emissions come from closed loops in which hot plasmas are confined, while it is not obvious whether the extended source at the initial phase comes from so-called "loops." Optical footpoints, which appear synchronously with the hard X-ray spikes, show nonsymmetric and

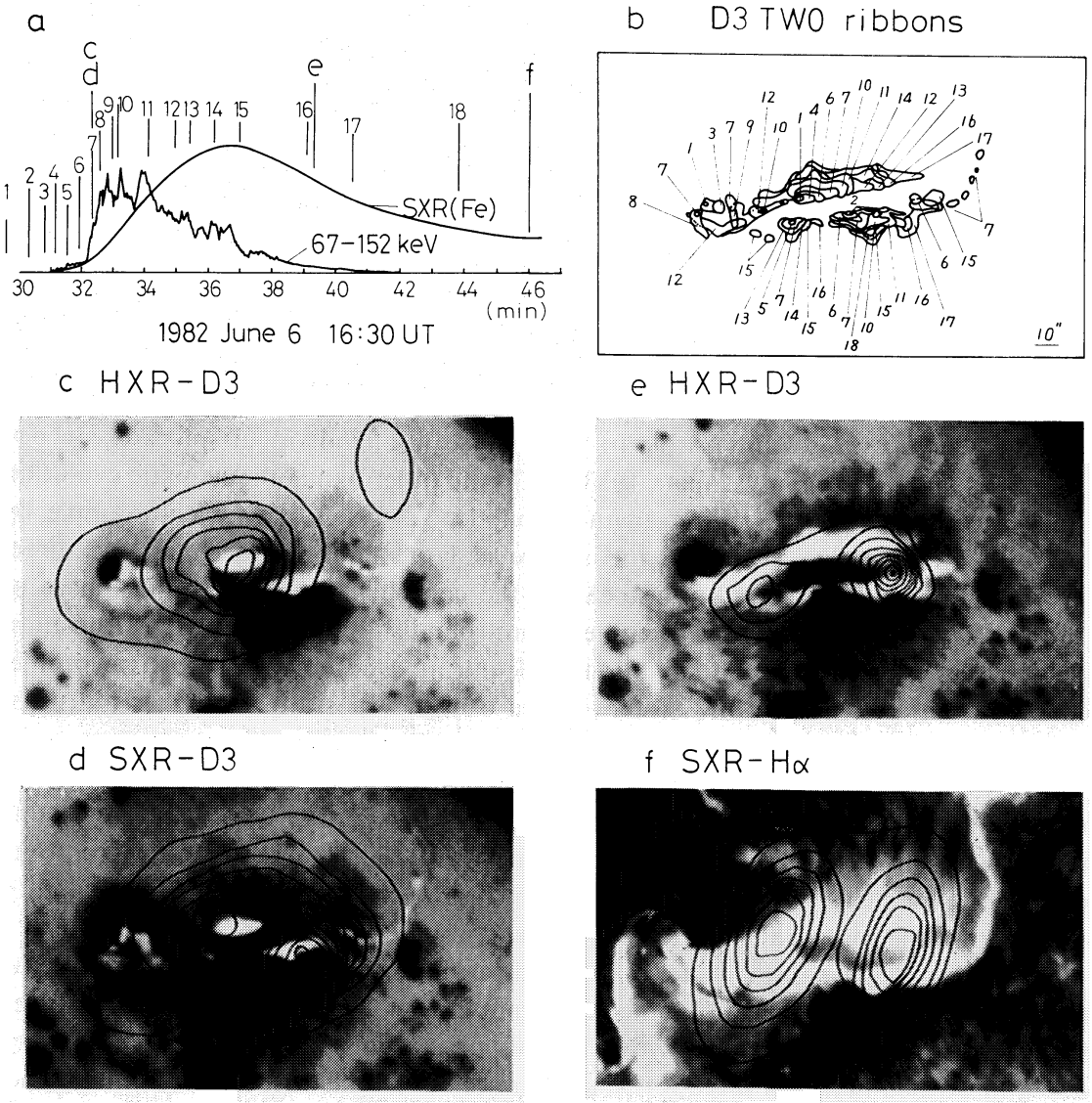

Fig. 2. Time profiles and morphology of the 1982 June 6 flare (X12 class). (a) Time profiles of SXR (total Fe-line count) and HXR together with various timings for b–f, (b) evolution of two-ribbon loci from He I D3 filtergrams, (c) and (e) HXR (25–35 keV) contour maps overlaid on D3 filtergrams, (d) and (f) SXR (6–13 keV) contour maps overlaid respectively on D3 (d) and Hα (f) filtergrams. Here c and d refer to the early impulsive phase and e and f refer to the later phases. Original pictures are from TZ85 (rearranged by the author).

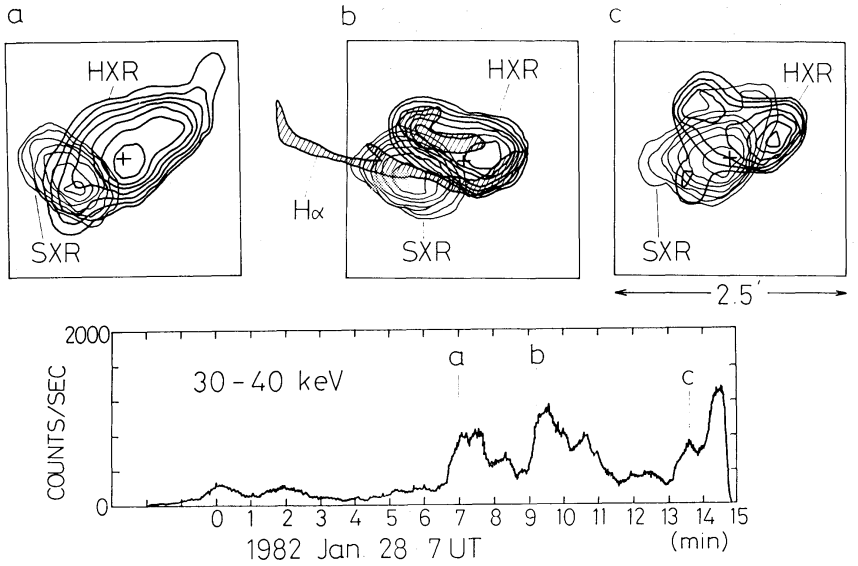

Fig. 3. SXR (6–12 keV, thin line) and HXR (25–35 keV, thick line) contours at three phases of a very hard event of 1982 January 28. Time profile is shown in the lower panel. Note the remarkable differences between SXR and HXR morphology. The Hα two-ribbon contour (courtesy of Beijing Observatory) is shown in b. The solar limb is directed to lower left corner. Original X-ray maps are supplied from Dr. T. Takakura.

irregular distributions and development on two sides of the inversion line; as can be seen in figure 2b conjugate footpoints show generally different shapes and sizes; plural footpoints on one side correspond to a common footpoint on the other side; brightening often repeats around the same footpoint region with different irregular shape to each other. There appear no Hα postflare loops connecting these early irregular footpoints. These features would not imply a symmetrical arcade structure of loops but suggest more disordered complexly sheared magnetic structures which are spatially intricate, bifurcating from common footpoint(s). They possibly appear transiently associated with the prominence eruption and do not persist as the flare loops. The two ribbons that develop in the main flare phase, on the other hand, are successively connected by symmetrical arcades of loops whose orientation is generally less sheared (or more perpendicular to the inversion line) towards later phases (cf. Zirin and Tanaka 1973). This evolution of the postflare loops implies successive formations of higher loop arcades in the course of flare. Figure 3 illustrates HXR morphology extremely different from the SXR loops in the impulsive phase of a particularly hard event. The SXR source is compact and stationary just above major part of the two ribbons, while the HXR source extends over the whole two ribbons and shows exceptionally striking changes in shape with a time scale of 10 s. Note in figure 3c that the SXR peak is located at depressed portion of the HXR contour suggesting loop top and footpoints for respective sources.

Hinotori observed many limb flares that provided good height information on the HXR sources. Figure 4 shows the flare of 1981 July 20, whose time profile is given in figure 1c (Tsuneta et al. 1983; K. Tanaka 1983). During the initial 6 min of the impulsive phase which lasted for 8 min, the HXR source showed a double structure.

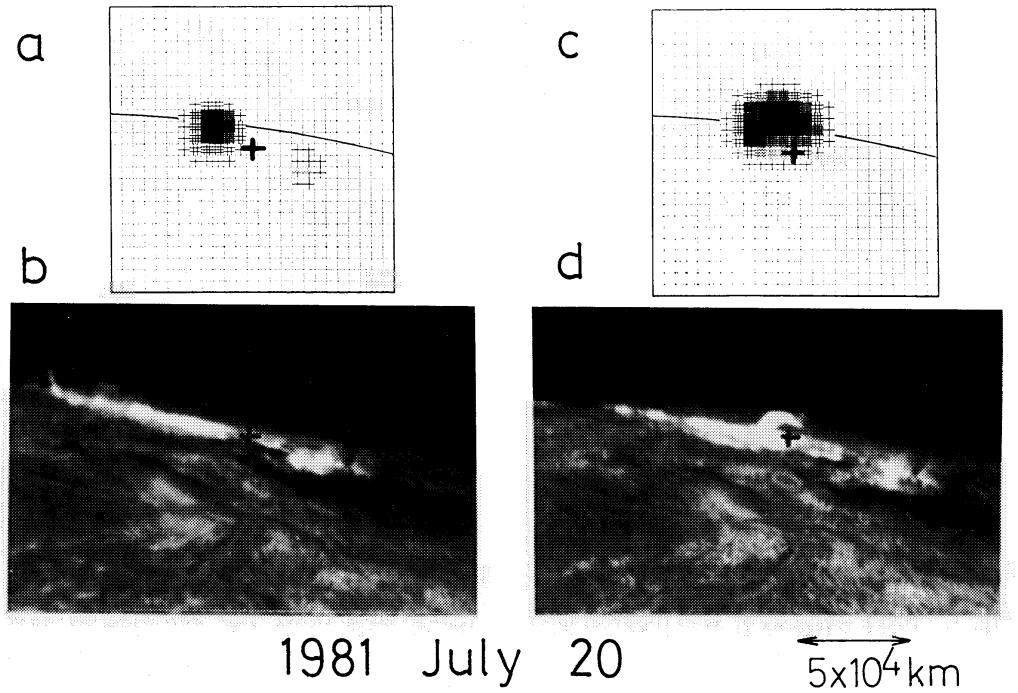

Fig. 4. The HXR maps (a, c) and Hα filtergrams (b, d) at early (a, b) and later (c, d) phases of the 1981 July 20 flare. Time profiles are shown in figure 1c. The same scale and orientation are used for all pictures (Hα pictures cover wider region than HXR maps). Solar limb and common reference point are given. The HXR data from Tsuneta et al. (1983) and the Hα data from Tel Aviv Station of the Big Bear Solar Observatory.

This was originally regarded as two footpoints. However, the main source extending from below to 15000 km above the limb is better identified with a composite of loops and footpoints as evidenced by the appearance of Hα loop system at this position with a long time lag. The HXR contour peak is located in the coronal region. The weaker subsource, 50000 km away from the main source, could be identified with an Hα bright footpoint region isolated from the main flare region. This subsource disappeared during the impulsive phase and when the burst entered the gradual phase, a different coronal source appeared suddenly at about 20000 km above the limb at a location between the double sources (figure 4c). The main source remains faintly visible. This new source agrees closely with a very bright Hα loop (figure 4d) that appeared 5 min later and displaced from the main loop ensemble described above. Obviously a new loop is activated in the gradual phase at a different place and emits the hard X-rays. One of the strongest proton events observed by the Himawari satellite coincided with this phase (N. Nitta 1986, private communication). This gradual phase is characterized by a hard spectrum ($\gamma=4.8$) with absence of the Fe XXVI emitting hot thermal component and presents one example for the quasi-thermal component. The weak subsource detached from the main extended source like this case has been observed in 8 events of 30 (TTH84). However, there is no definite case confirming that double sources are concentrated at two conjugate footpoints. Some limb flares show the main source detached from the limb and subsource inside the disk. The latter disappears towards the end of the impulsive phase and could be identified with the footpoints (Ohki et al. 1983; also see, e.g., figure 13).

Figure 5 shows another limb event with very hard spectrum ($\gamma=2.6$–3) (1982 January 22; Takakura et al. 1987). The HXR emitting region extends from the two Hα ribbons located very close to the limb to 10000 km above the limb. In the early phase the SXR sources are concentric with the HXR sources but considerably smaller

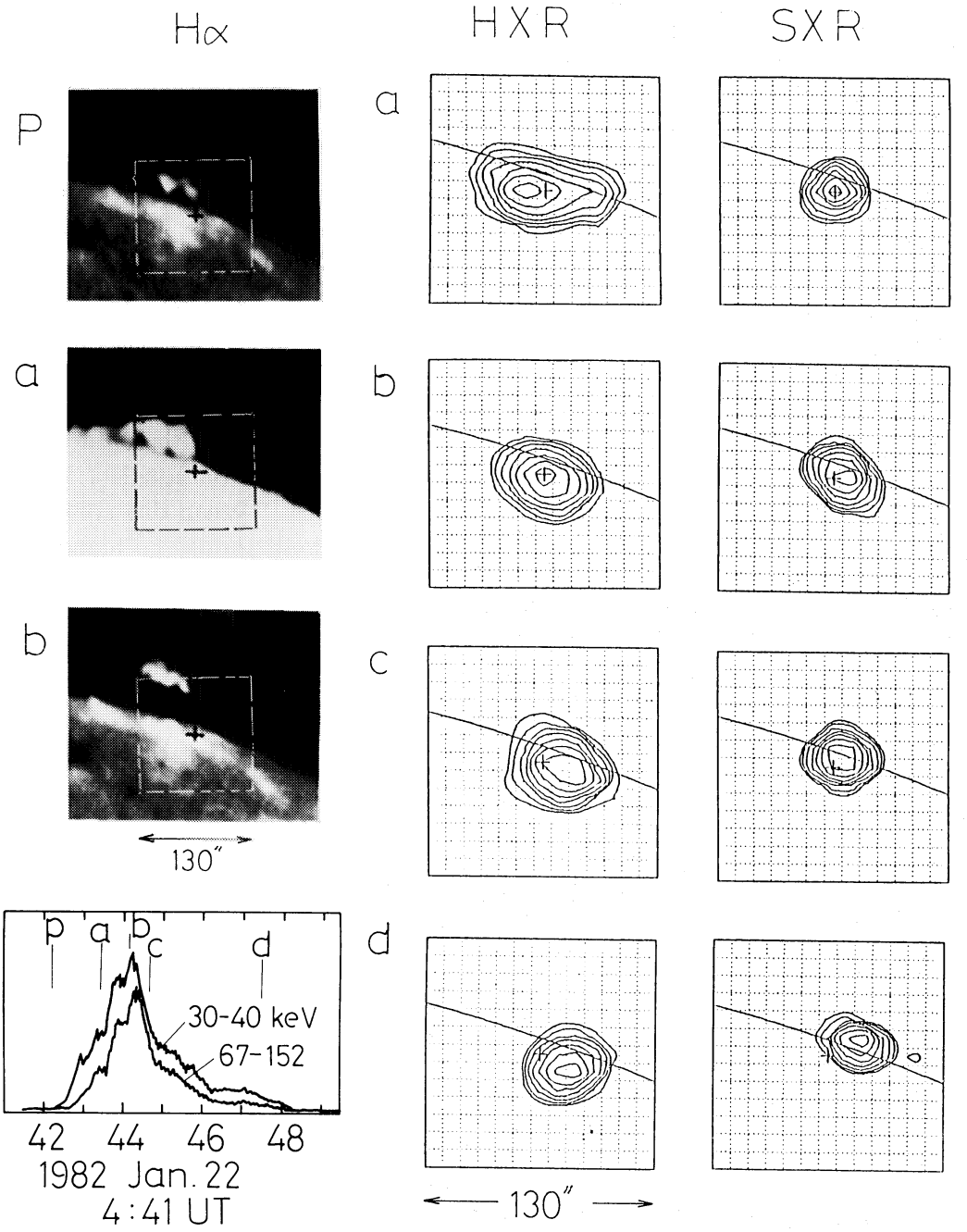

Fig. 5. The limb event of 1982 January 22. The HXR time profiles, HXR (25–35 keV) and SXR (6–12 keV) images, and Hα pictures (from Mitaka) are shown. The cross marks in Hα denote the centers of the X-ray maps. Note that the centroid of X-ray source is located at one foot of the erupted prominence. A rising prominence is shown in upper portion of frame b (Hα). Original data from Takakura et al. (1987) (rearranged by the author).

than the latter. In this phase the SXR band (6–12 keV) is contributed significantly (30–80% of the total flux) by the impulsive component, though it is dominated by the SXR thermal component later. The centroids of the two sources are located slightly above the inversion line but well below the erupting filament suggesting a very low site for the initial energy release, presumably just above the chromosphere. The HXR source shows a shift along the limb in accordance with that of the brightest part of the two ribbons, but shows no upward shift that was clearly observed later in the SXR source (figure 5, frames c, d of SXR). This is a rather exceptional case in which the HXR source is not cospatial with the SXR source even in late phase.

These examples indicate that the major HXR emission at 20–30 keV comes from the extended coronal region and contribution from the footpoints is minor. This result would not contradict the thick-target nonthermal model, because the thick-target condition is realized in the corona due to unexpectedly high ambient densities. Analysis of density-sensitive X-ray line ratios (Doschek et al. 1981) shows that the preflare coronal density is at least 2×10^{10} cm^{-3}. Mean density derived from the SXR source size and emission measure at the onset of the burst is $10^{10.4}$ cm^{-3} for a very large flare (TZ85) and $10^{10.5}$ cm^{-3} for a small flare (Takakura et al. 1987). This density increases to 10^{11} cm^{-3} and to $10^{10.8}$ cm^{-3}, respectively, for these flares. With these densities the mean free path of a 20 keV (30 keV) electron equals 1.5×10^{4} km (4×10^{4}) km without taking account of the spiraling effect. When due consideration is given to the filling factor, the actual density of the loop should be higher. Thus the electrons are mostly dissipated within the loops and, only in the most favorable case of short loops and low density, may possibly reach the footpoints.

Takakura (1986) performed numerical simulations for the dynamics of nonthermal electrons injected at the top of a model coronal loop. By solving the Fokker–Planck equation he obtained the spatial and temporal distribution of the HXR emission and examined the effects of the loop density, injection period, initial pitch angle distribution, and tapering of the magnetic loop. The most important parameter that affects the footpoint versus loop contrast proved to be the loop density. For a fixed loop length of 3×10^{4} km, the derived brightness contrast of the footpoint to the loop top in 20-keV X-rays is 4–5 for $n=10^{10}$ cm^{-3} and 0.5 for $n=5\times10^{10}$ cm^{-3}. At 60-keV X-ray this contrast increases to 10–50 and 1.5–2 for these respective densities. The observed broad extension ($2–3\times10^{4}$ km) of the HXR source at 20–30 keV without clear brightening at boundaries seems to be compatible with these simulations in high density at the present spatial resolution (about 7000 km). The low contrast (10–20%) of the possible footpoint sources which are found in the extended source or in the subsources is thus reasonable. The SMM HXIS observations of the footpoint emission also show low contrast (Hoyng et al. 1981; MacKinnon et al. 1985). The footpoint emission would be more apparent if observed at higher-energy X-rays.

Indirect but more convincing evidence for footpoint excitation by high-energy particles may be derived from the precise synchronism of the optical flashes at footpoint locations with the HXR spikes. Fast sequential brightenings in Hα and other optical bands simultaneous with HXR spikes had already been noted in the observations during the previous cycle as evidence for the particle bombardment (cf. Vorphal 1972). In particular, fast flashes at 3835 Å in the 1972 August 2 event (Zirin and

Tanaka 1973) showed pair brightenings at different points along the neutral line with a time scale of 10 s, coincident with the individual HXR spikes and suggested that the burst sequence comprises elementary bursts occurring sequentially at different loops. The flashes are sharply bounded in small areas, less than 0".5 (360 km) in some cases, implying very small cross sections of the loops in which acceleration takes place. The SMM UVSP observation in terms of Si IV line (Cheng et al. 1981) provided further evidence for this picture with a better temporal resolution of 4.6 s (spatial resolution 4"). High resolution Hα observations at the Hida Observatory detected remarkable simultaneity within 1s for the impulsive brightenings at the distant footpoints of opposite polarity coincident with the HXR spikes (Kurokawa et al. 1986; Kurokawa 1986). The thermal conduction or X-ray illumination could not explain such precise time coincidence at sharply bounded footpoints. The electron beam excitation is also suggested from the analysis of broad Hα line profiles (Canfield and Gunkler 1985).

The thermal versus nonthermal arguments for the origin of the impulsive component remain controversial. The extended HXR source structure with its peak located at the coronal region and without enhanced boundaries may support the thermal model, but this feature seems also compatible with the nonthermal model. On the other hand, other facts appear not to favor the thermal model. In the flare of 1981 July 20 (figure 4), which showed a distant (50000 km) subsource identified with the footpoint, a propagation of the emission with a velocity of ~ 1000 km s^{-1} should be expected in the thermal model but was not observed with a time resolution of 8 s. In the limb flare of 1982 January 22 (figure 5) the source size of the impulsive component is smaller in the lower-energy band (6–13 keV) than in the band of 25–35 keV; the two image contours are similar and the peaks coincide. This may be interpreted to support the nonthermal beam model as the lower-energy electrons dissipate in shorter distances, whereas by the thermal model a temperature distribution would result along a loop, which predicts a larger size in the softer band (Takakura et al. 1987).

As described the evolution of the HXR source structure in the postmaximum phase has many facets. Most cases show a transition of the source to a more compact, coronal source identified with the SXR loops and the optical postflare loops. This transition occurs in some cases progressively to higher altitude with a velocity of tens of km s^{-1}, while the impulsive time profile continues. In others, it occurs abruptly with the onset of the gradual phase. It corresponds to a phase in which the two ribbons separate progressively away from the inversion line after spreading along the neutral line. It is conceivable that the energy release site shifts from the low-lying sheared magnetic fields in the impulsive phase to successively higher magnetic fields anchored at distant footpoints. The fact that the two ribbon separation occurs in a more localized portion of the inversion line than in the initial spreading of Hα may explain a shrinking of the HXR source size along the inversion line. The gradual phase of the impulsive flare resembles either the gradual-hard flare or the hot thermal flare which are discussed later. Substantial cases are contributed by the hot thermal component which is confined near the loop top. Others are contributed by nonthermal emission from the electrons trapped in the corona as in the gradual-hard flare. Some flares, lacking the gradual phase, show no upward shift. They imply continued HXR

emissions from sources different from the SXR loops. One might infer that the evolutionary change to a higher compact source is caused by an increase in the ambient coronal density which reduces the dissipation length of electrons in the loop and hence reduces the source size. Chromospheric evaporation could be a candidate to cause this effect. However, the basis of this explanation, namely that the energy release continues in a single loop for more than 30 s during which evaporated matter spreads a loop, seems to contradict a more acceptable view that the energy release sites move to different locations with time. Nevertheless an evaporation-induced density increase at a site, where the electrons are to be produced, may be realized, if the SXR plasmas are produced in the same loop earlier than the hard electrons are produced, or if field-crossing diffusion of the evaporated material occurs.

4. Gradual-Hard Flares (Type C)

The gradual-hard flare (type C) is distinguished from the impulsive-type flare (type B) by its long-enduring, gradual HXR time profile lacking the spiky variations. The burst often lasts over 30 min showing one or more broad peaks of duration from one to 10 min. The impulsive phase appears either to be imperceptible (Tsuneta et al. 1984b) or to precede the main peaks by a long time of about 60 min (Dennis 1985). The HXR spectrum is generally harder than in the impulsive burst and is better fitted by the power-law than by the exponential distribution ($\gamma=2.5$–4; TTH84). It shows a progressive hardening with time through the peak(s). This type of burst is known as microwave rich in comparison with the HXR flux (Cliver et al. 1986; Kai et al. 1985; Dennis 1985). Kai et al. (1985) have shown that the peak flux at 17 GHz relative to the peak 67–152-keV flux is systematically larger in the burst of extended duration than in the short-duration impulsive burst. This microwave excess is attributed to an abundant population of the relativistic electrons in the extended burst. Association of the meter-wave type IV burst with the gradual-hard flare is also pointed out (Tsuneta et al. 1984b; Dennis 1985). The SXR characteristics show some contrast to those of the impulsive flares. Blueshifts of the emission line are either absent or very weak, and the line broadening is smaller and its temporal variation is less conspicuous. The SXR line and continuum emissions increase steadily during the HXR burst but their increase curves are uncorrelated with the HXR peak(s) (figures 1e and 6b). The electron temperature derived from the Fe XXV line ratio has rather constant, low values below 2.5×10^7 K with no increase associated with the burst peak as seen in the impulsive flares. The emission measure is either stationary or slowly increases with time during the burst. The Fe XXVI emission is generally weak and the hot thermal component of $T>3\times10^7$ K is insignificant except in the case of one behind-the-limb event on 1981 April 27 (Tanaka 1986b).

This type of flare seems to have occurred more frequently in the 1981 period of Hinotori operation than in the 1980 period of SMM HXIS operation, due possibly to a change of the flare type according to the phase of solar cycle. Consequently Hinotori obtained X-ray images for many of the gradual-hard flares (seven flares of 30 are classified as this type; TTH84). Four events were examined in detail, of which the 1981 May 13 flare studied by Tsuneta et al. (1984b) is regarded as a standard type.

The major difference in the HXR morphology as compared to the impulsive flare is a large extension and high altitude of the source throughout the flare period. The source is detached from the surface and its centroid is located at heights ranging from 2×10^4 km to 9×10^4 km. The source size at FWHM is 20″ for the 1981 April 27 flare (Takakura et al. 1983c) and 70″$\times$30″ for the 1981 May 13 flare and 1981 April 1 flare (Takakura et al. 1984b), and is thus clearly beyond the instrumental resolution. Moreover the source is rather stationary during its long period, though some minor changes certainly occur. Comparisons with the magnetic lines of force derived from the potential field calculations by Sakurai (1983, 1985) reveal that the sources are located at the ridge of high coronal loop arcade. The magnetic field strength at the source region is not high, being on the order of 50 G, and by combining this value with a typical electron temperature of 2×10^7 K and electron density of 3×10^{10} cm^{-3}, a plasma beta value at the source is estimated to be equal to unity (Tsuneta et al. 1984b). It has been demonstrated that for the HXR peaks, at least 40% of the total counts in the HXR images is contributed by the power-law component (Tsuneta et al. 1984b; Takakura et al. 1983c). Thus the extended sources high above the surface are believed to indicate the presence of a rich population of high-energy electrons with a power-law spectrum in the coronal loop arcade. Interferometric observations at microwave wavelength, although one dimensional, support the presence of MeV electrons at the same coronal location as the HXR sources (Kawabata et al. 1983). The SXR images at 6–13 keV were obtained in later phases when the HXR spectrum is hardest. They nearly accord with the HXR sources except for a small (less than 10″) displacement of the centroid found for some events (e.g., May 13 flare) and slightly larger extensions.

The stationary HXR sources and prolonged peak may suggest a trapping of the high-energy electrons in the coronal loops. Bai and Dennis (1985) tested a perfect-trap model for the May 13 event. The observed spectral hardening was reasonably explained by the energy-dependent decay of electrons for an ambient density equal to 5×10^8 cm^{-3} in the trap model. But this contradicts a mean ambient density of 3×10^{10} cm^{-3} derived from the SXR (Tsuneta et al. 1984b). For this density the resulting spectral index should remain almost flat. The result instead suggests a continuous energy injection of the high-energy electrons at the source location during the extended emission peak. Continuous energy injection is also necessary to balance a high and steady conduction loss rate (1.1×10^{29} erg s^{-1}) from the source to the lower atmosphere. With the derived high ambient density, low-energy (10–30 keV) electrons dissipate immediately at the source region, and their thick-target energy loss (2×10^{29} erg s^{-1}) deposited in the source consistently explains the conduction loss (Tsuneta et al. 1984b).

The evolution of the 1981 May 8 flare provides an excellent example which shows a progressive, though small, movement of the HXR source in accordance with an Hα two-ribbon development. As shown in time profiles (figure 6b) this event presented three prominent HXR peaks, each having a FWHM duration of about 2 min, and systematic hardenings of the spectrum (typically γ decreases from 5 to 3.5) have occurred associated with each of the three peaks. The HXR source shows an extended structure centered at the top region of Hα loop arcades which appeared later (figures

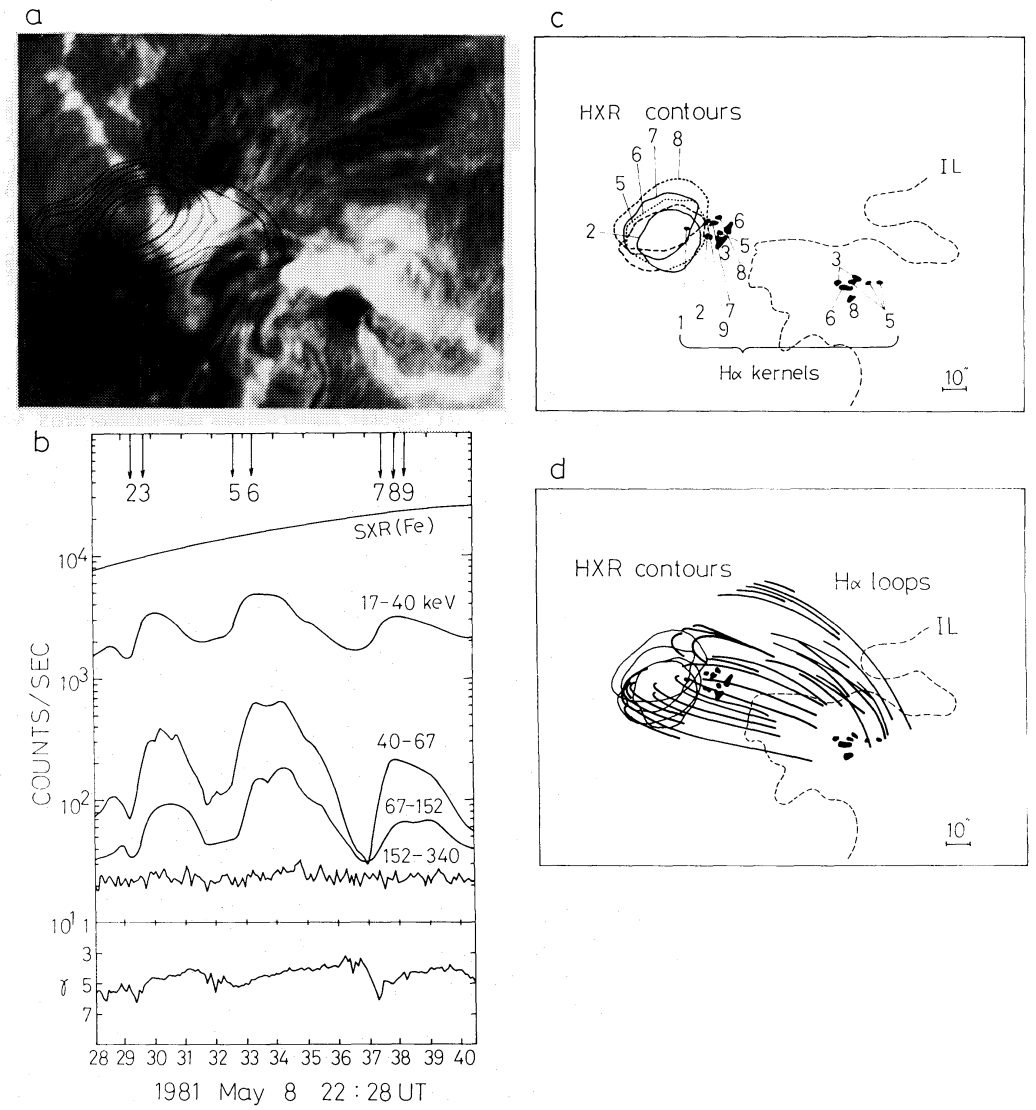

Fig. 6. The gradual-hard flare of 1981 May 8. (a) An overlay of HXR (17–35 keV) contour on Hα filtergram at 22: 38: 05 UT, (b) time profiles of SXR Fe-line flux, HXR fluxes in four channels, and power-law index (γ) of the HXR spectra (>40 keV), (c) developments of Hα two-ribbon kernels (in off-band pictures at 1 Å from the center line) and HXR source (given by the contour at 56% of the peak) with corresponding times indicated by arrows in (b), where IL denotes the inversion line, and (d) Hα post-flare loops overlaid on the HXR sources and two-ribbon kernels shown in (c).

6a and 6d), though there appeared a second weaker HXR source at some phase. The Hα observation made at the Big Bear Solar Observatory completely covered this extremely long (2.5 h) flare and confirmed a very slow start of the Hα flare without filament eruption and impulsive brightening. At the start of the flare the two ribbons are already separated at large distance (75″) and show irregular expansion jumping from one place to the adjacent with a time of 1–3 min and crossing umbrae of opposite polarity. At the leading edges of the two expanding ribbons there appeared small (3″) Hα kernels (seen in Hα±1-Å filtergrams), whose successive movements are correlated with the systematic displacements of the major HXR source contours as shown

in figure 6c. The displacements during individual HXR peaks are minor but during two consecutive peaks they are conspicuous. This clearly indicates progressive activations of different loops with different associated footpoints in the course of the HXR burst. The footpoint, with a typical size of 3″, shifts to adjacent (within 10″) places in two or three steps during individual peaks, and jumps to another place when a different HXR peak appears. The appearance times of the different kernels are indicated by arrows in the HXR profile (figure 6b). In periods between two consecutive HXR peaks the kernels disappear but diffuse two-ribbon emissions in extended area are present together with the HXR stationary source. The HXR emissions appear to be contributed by two portions of the loop arcade; the peaks are mainly contributed from thin loops whose footpoints are concentrated in the small front kernels, and the background emissions come from a large ensemble of loops with footpoint corresponding to the two extended ribbons. The background emissions amount to 30–50% of the peak emissions. The whole system of the loops is progressively replaced by higher systems as the flare proceeds. This example implies that, even within a single peak, the HXR is emitted successively from different loops located adjacently, and hence the spectral hardening occurs for the HXR emissions from different loops. A progressive acceleration may be suggested as the electrons drift successively from loop to loop. The estimated height of the loops in which the electrons are spiraling increases from 6×10^4 km to 9×10^4 km during a 20-min period. The increase during the individual peaks is an order of $1\text{–}2\times10^4$ km. The SXR sources are similar to the HXR sources but slightly more extended to lower height. The mean ambient density is about 3×10^{10} cm^{-3}.

The apparent upward shift of the source described above may be present in other gradual-hard flares, presumably, with a reduced rate. But a significant detection would require a higher spatial resolution and a longer time coverage. Similar source motions have been observed in the gradual phase of the impulsive flare for some HXR images and, more generally, for the SXR images as discussed later. However, the geometrical heights and extensions are much smaller in the case of the impulsive flares.

5. The Thermal X-Ray Emissions

5.1. Spectroscopic Diagnostics of Hot Flare Plasmas

(a) Electron temperatures

The high-resolution SXR spectra from highly-ionized metal ions were studied extensively by the Bragg spectrometers flown on P78-1 (Doschek et al. 1979), SMM XRP (Culhane et al. 1981), and Hinotori (Tanaka et al. 1982a). Two quartz crystals aboard Hinotori obtained high-resolution Fe spectra in regions of 1.82–1.89 Å and 1.73–1.95 Å with a temporal resolution of 8–11 s. These experiments enabled precise determinations of the electron temperatures of hot flare plasmas from the He-like or H-like resonance to dielectronic recombination line intensity ratios for the ions of Fe and Ca. The electron temperatures derived from the He-like iron are systematically higher (by $3\text{–}6\times10^6$ K) than those derived from the He-like calcium (Doschek et al. 1980; Feldman et al. 1980a, b) indicating some range of temperatures. The electron temperatures from the iron are already $15\text{–}20\times10^6$ K when the high-resolution Bragg

spectrometers provide spectra of significant statistics, increases to a range of 20–27$\times$ 10^6 K in a few minutes, and decreases more slowly to the value around 20×10^6 K. In many flares the amplitude of T_e variation is within a few million degrees. Only lower resolution spectra obtained from one of the spectrometers aboard Hinotori and from Tansei IV (Tanaka 1980) indicate spectra of $12–15\times10^6$ K at the initial phase.

One of the Bragg spectrometers aboard Hinotori provided a number of Fe XXVI (H-like) spectra with significant count statistics (Tanaka et al. 1982a, d; Moriyama et al. 1984). This allowed detailed electron temperature diagnosis for the hottest part of the flare plasmas. Applying a profile fitting technique (cf. Parmar

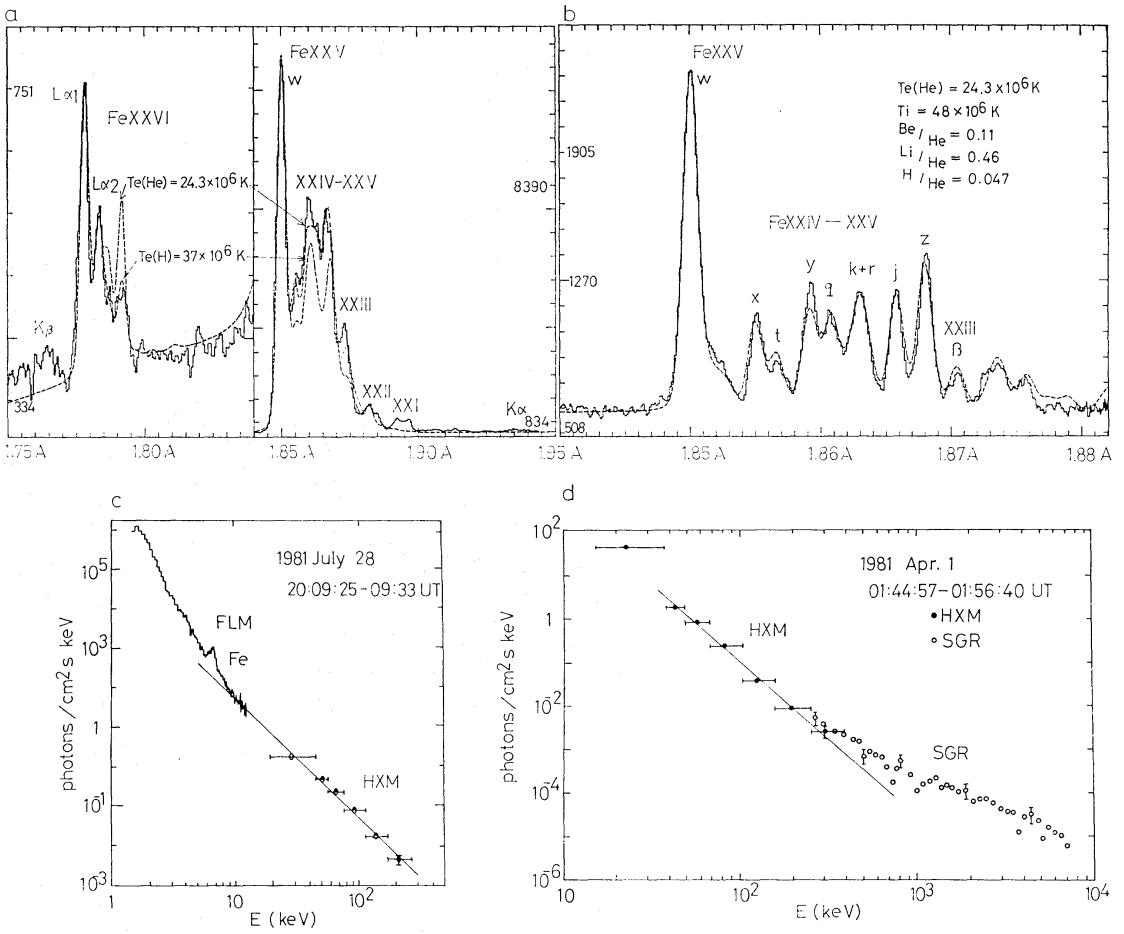

Fig. 7. SXR to γ-ray spectra observed by Hinotori. (a) Fe-line spectrum at 1.75–1.95 Å from the lower-resolution Bragg spectrometer. Two theoretical fits (dash line) are shown. Note that Fe XXVI is fitted by $T_e=37\times10^6$ K, while Fe XXV–XXIV is fitted by $T_e=24.3\times10^6$ K; 1981 October 7 flare, 23: 0: 8–23: 1: 18 UT (cf. figure 8a). (b) Fe XXIII–XXV line spectrum at 1.84–1.88 Å from the higher resolution spectrometer. Theoretical fit with $T_e=24.3\times10^6$ K is shown. (c) Combined SXR and HXR spectra respectively from the scintillation proportional counter (FLM) and the scintillation counter (HXM). Fe-line complex at 6.7 keV is resolved. A power-law fit is shown at 7–200 keV. (d) Combined HXR (HXM) and γ-ray (SGR) spectra from 17 keV to 7 MeV. Here (a) and (b) are from Tanaka (1986b), (c) from Tanaka et al. (1984), and (d) from Yoshimori et al. (1985).

et al. 1981; Antonucci et al. 1982) to the Fe XXVI spectrum at 1.77–1.80 Å which is composed of Lα lines and many blended di-electronic recombination satellites (Dubau et al. 1981), the electron temperature could be determined with an accuracy of 2×10^6 K independent of the ionization balance (Tanaka 1986b). Figure 7a shows an example of such fitting. The electron temperatures thus derived [denoted as T_e (XXVI) to distinguish the electron temperatures from the He-like spectrum, T_e (XXV)] have led to an important finding of a higher temperature component above 3×10^7 K in a substantial number of flares (Tanaka et al. 1982d; Moriyama et al. 1984; Tanaka 1986b). This superhot plasma designated as the hot thermal component has been discovered independently by Lin et al. (1981) in the high-resolution continuum spectra (above 10 keV) of a flare. Tanaka (1986b) has shown, from a study of 13 large flares, that T_e (XXVI) increases from about 20×10^6 K in the early phase to $31–40\times10^6$ K (five flares) and to $22–27\times10^6$ K (six flares) in the flare peak. T_e (XXVI) deviates from T_e (XXV) by $7–13\times10^6$ K in the former "high temperature" group and by less than

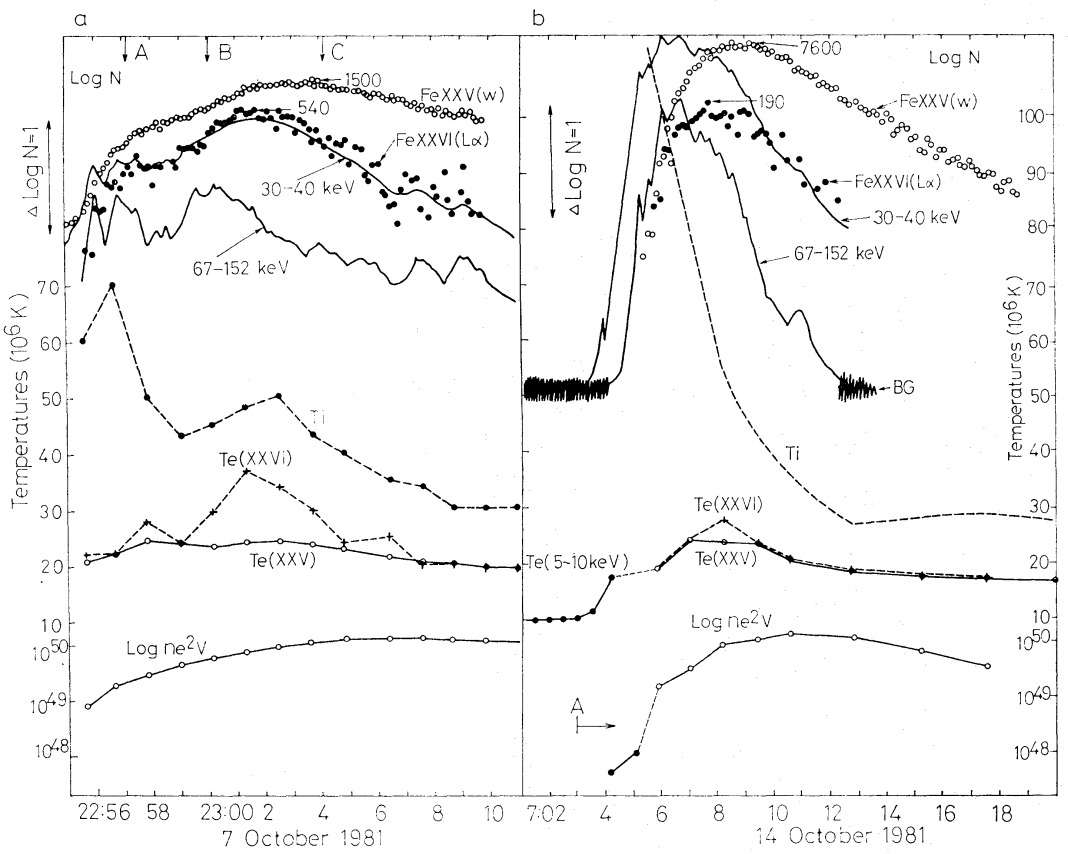

Fig. 8. Time profiles of SXR and HXR fluxes for various plasma parameters for two types of flare. [(a) Impulsive flare with enhanced hot thermal component and (b) typical impulsive flare.] T_i: ion temperature denoting Doppler line broadening, T_e (XXVI) and T_e (XXV): electron temperatures derived respectively from Fe XXVI and Fe XXV spectra, n_e^2V: emission measure from Fe XXV intensity. The fluxes are shown by the same logarithmic scale so the relative variations may be compared. From Tanaka (1986b). Preburst increases in electron temperature and emission measure from the continuum spectra (5–10 keV) are also indicated in (b). The letter A marks the start time of a slow emission measure increase.

4×10^6 K in the latter "low temperature" group. T_e (XXVI) agrees generally with T_e (XXV) in later phases. The T_e (XXVI) increases occur in 1.5–2 min and the T_e (XXVI) decrease to the level of T_e (XXV) occurs in 3–7 min. Figure 8 gives two cases of temperature histories in comparison with the SXR and HXR flux profiles. Figure 8a (high-temperature flare) shows an increase of T_e (XXVI) by 13×10^6 K without an increase of T_e (XXV) during a pronounced peak in the Fe XXVI Lα time profile. The HXR flux at 30–40 keV shows, after a weak impulsive phase, a major enhancement whose time profile is quite similar to the Lα profile. Actually the HXR emissions are explicable in terms of T_e (XXVI) and related emission measures, confirming the identity of the two sources. Figure 8b (low-temperature flare) shows neither an appreciable increase in T_e (XXVI) nor a large deviation between the two temperatures. The HXR profiles show impulsive variations only. Generally the impulsive flare without a gradual enhancement in later phases shows the "low temperature" characteristics like figure 8b. In these figures are plotted ion temperature (T_i) denoting Doppler line broadening. The large deviation of T_i from T_e (XXVI) in the early phases may exclude a possibility that T_i represents a higher electron temperature component. Figure 9a gives a correlation diagram of peak values of T_e (XXVI) and T_e (XXV) against the peak fluxes in 1–8 Å observed by GOES. Obviously the peak T_e (XXVI) distribution bifurcates into two groups. The low T_e (XXVI) group merges with a distribution of the

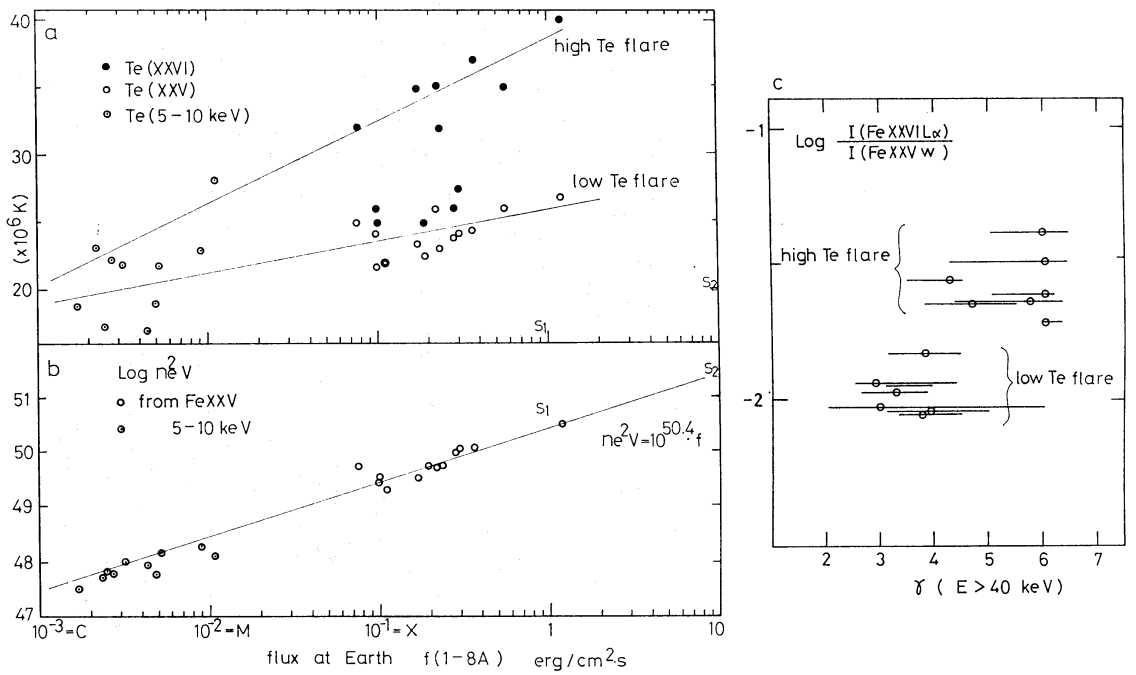

Fig. 9. Various correlation diagrams. (a): Peak electron temperature versus peak SXR flux (1–8 Å) from the GOES (three kinds of temperatures are shown). (b) Peak emission measure versus peak SXR flux. C, M, and X denote respective X-ray class. s_1 and s_2 represent flare stars (s_1: Proxima, 1979 June 3 and s_2: YZ CMi, 1979 October 25). (c): Peak intensity ratio of Fe XXVI to Fe XXV (relative significance of the hot thermal component) versus range of power-law index (γ) of HXR (>40 keV) spectra. Circles denote the index at the peak flux. (a) and (b) are from Watanabe (1984b) with supplement of data from Tanaka (1986b) and HXR spectral data from N. Nitta (1986, private communication).

peak T_e (XXV). The low T_e (XXVI) flares are all characterized by distinct impulsive component with hard HXR spectrum (figure 9c).

The emission measures derived respectively from Fe XXV and XXVI line intensities assuming ionization balances at respective electron temperatures are comparable and are both large, exceeding 10^{49} cm^{-3} at the peak. This fact, coupled with the large T_e (XXVI)$-T_e$ (XXV) differences in the "high temperature" flares, argues for a broad peak of the temperature distribution of the plasma extending from 20×10^6 K to over 40×10^6 K at the peak of the "high temperature" flares (Tanaka 1986b). T_e (XXVI) and T_e (XXV) represent mean temperatures of this broad distribution weighted by respective contribution functions, and large amplitude of the T_e (XXVI) increase results from higher sensitivity of the Fe XXVI contribution curve to higher temperatures. The fact that T_e (XXVI) and T_e (XXV) are both well below the temperatures giving maximum contribution (respectively, 10^8 K and 6×10^7 K) implies the dominance of relatively lower-temperature plasmas ($<5\times10^7$ K) in the flare. The substantial heating manifested in the T_e (XXVI) increase can be found in the peak phase of some 50% of the impulsive flares, which show gradual HXR ($E<40$ keV) emission originating from the same plasma component. The rest of the impulsive flares have less significant population of plasma above 30×10^6 K, and the temperature distribution has a plateau at $T_e=20$–25×10^6 K. The higher T_e component above 3×10^7 K appears to be generated preferentially at higher altitudes from the start of the flare. This is evident not only from the behind-the-limb events which showed exceptional large and persistent deviation of T_e (XXVI) from T_e (XXV) from the beginning through most of the period (Tanaka 1986b), but also from the compact thermal HXR sources located near the loop top as discussed later.

Various multi-temperature structures have been explored to explain consistently the emissions from Fe XXVI, Fe XXV, and lower ionization stages in a scheme involving a homogeneous atmosphere with ionization equilibrium. A two-temperature model (Tanaka et al. 1983) leads to two components, respectively, with $T_1>T_e$ (XXVI) and $T_2<T_e$ (XXV). For an X12 flare T_1 ranges 30–50×10^6 K and T_2 ranges 13–20×10^6 K with emission measures for T_1 being about one order of magnitude smaller than those for T_2. In a differential emission measure approach (Akita et al. 1982), an emission measure peak initially develops around 20×10^6 K and broadens to higher temperatures with the wing extending to 5×10^7-K region. The higher T_e wing shrinks promptly, and later cooling proceeds isothermally and slowly at constant emission measure. These approaches, however, have been confronted with a difficulty of apparent violation of the ionization equilibrium between Fe XXVI and Fe XXV. F. Moriyama (1984, private communication), Akita (1985), and Tanaka (1986b) have found that the H-like ion is significantly overpopulated compared with the existing ionization balance models, especially, in the initial and decay phases where T_e (XXVI)$=T_e$ (XXV) prevails (figure 10). Akita (1985) and F. Moriyama (1984, private communication) have shown that the multi-temperature distributions cannot resolve this discrepancy. Non-equilibrium condition might be suspected; but as argued by Tanaka (1986b) a long-lasting recombining condition is unrealistic in view of the high density (recombination time at $n_e=10^{11}$ cm^{-3} is 10 s). Other possibilities such as electron-impact ionization and photoionization can reasonably be excluded. This puzzling situation may in-

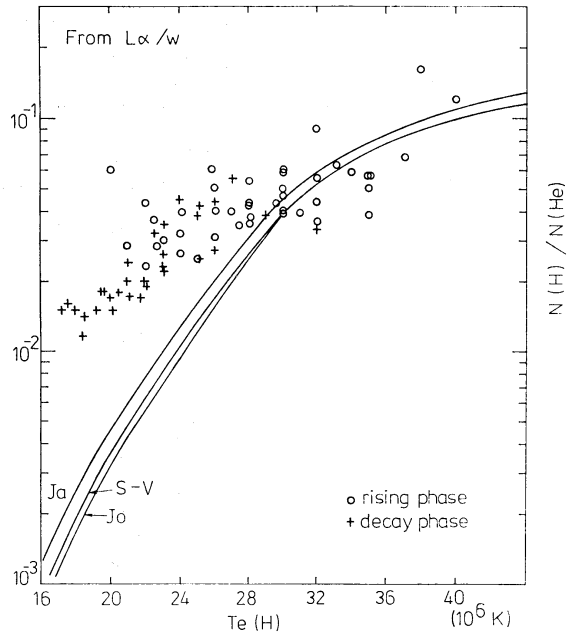

Fig. 10. Empirical ionization balance between Fe XXVI (H-like) and Fe XXV (He-like). H-like to He-like population ratios are plotted against electron temperatures from Fe XXVI spectra. Theoretical ionization balance is shown for the models of Jacobs et al. (1977; Ja), Jordan (1970; Jo) and Shull and Van Steenberg (1982; S-V). Reproduced from Tanaka (1986b).

dicate a real problem in the atomic physics though it is hard to expect serious inaccuracy in the atomic data for such simple ions. Further exploration would need to take account of different spatial distributions for the higher and lower T_e plasmas and nonequilibrium condition(s). For the lower ionization stages a persistent deviation from the equilibrium was first pointed out between the He-like and Li-like ions of Ca and Fe (Doschek et al. 1979; Tanaka et al. 1982d). More recently, using combined data from the SMM XRP and Hinotori, Antonucci et al. (1984a) have derived empirical relations for the ionization balances, respectively, between Fe XXV and Fe XXIV and between Fe XXV and Fe XXIII, which are consistent in the two data sets and do not depend upon the flare phase. The results are within a large scatter of existing ionization balance models and so may be compatible with the equilibrium.

Some evidence of weak transient ionization is found in some very early-phase spectra from the lower-resolution spectrometer on Hinotori. As discussed by Doschek and Tanaka (1987) the spectra showed an enhancement of inner-shell excitation line q(Fe XXIV) resembling the calculated transient spectrum at a time of 3s after the onset of heating (at $n_e = 10^{11}$ cm^{-3}). Initial heating may have been detected in the LiF spectrometer aboard the Tansei IV satellite which had an order-of-magnitude higher sensitivity compared to other high-resolution spectrometers though the resolution was low (0.01 Å). Coincident with or slightly earlier than microwave burst, initial enhancement occurred at Kα and around 1.9 Å (Fe XX) and subsequently shifted in less than 10s to 1.86 Å region (Fe XXIV), indicating that the ionization proceeds at high ambient density of about 10^{11} cm^{-3} (Tanaka 1980).

Reliable electron temperature diagnosis has also been provided from the high-

resolution continuum spectra obtained by a scintillation proportional counter aboard Hinotori. This type of detector, here flown on spacecraft for the first time, is able to resolve major emission lines (Ni, Fe, Ca etc.), since it has a factor two better resolution than the conventional proportional counter (figure 7c; Inoue et al. 1982), and thereby achieves reliable analysis of the continuum spectrum in the region 1.5–12 keV. Because of its very high sensitivity and consequent saturation problem, data reduction was restricted to small flares and early flare phases that could not be studied by the Bragg spectrometers. Watanabe et al. (1982, 1983) and Watanabe (1984a, b) have derived the following general characteristics for small flares (mainly SXR-class C); the electron temperature increase is limited to the period of the impulsive HXR burst, and the emission measure increases beyond the end of the burst and its peak lags the T_e peak by 0.5–3 min (X-class flares give time lag of 1–8 min). Rates of the decreases in T_e and the emission measure are much slower than those of the increases. The peak T_e is in the range $14–28\times10^6$ K. The highest T_e (28×10^6 K) may indicate a possible existence of the hot thermal component in a small class flare. As found from figures 9a and 9b the peak T_e is weakly correlated to the peak 1–8-Å flux over a three orders-of-magnitude range of flux, while the peak emission measure is nicely correlated to the peak flux over a four orders-of-magnitude range which includes flares from stars (Watanabe 1984b).

One interesting property found from the continuum analysis may be a slight T_e increase immediately before the HXR burst. It occurs from below 10^7 K to $12–15\times10^6$ K starting 30 s (smallest event) to 1 min (larger flares) prior to the HXR burst. An example is shown in figure 8b. These small but definite increases have been detected from the original spectra contributed from the full sun. When we subtract the preflare background spectrum as usually do for the analyses of flare spectra, the residuals become too small and the fluctuations too large to obtain reliable detection of such small temperature increases. This finding gives evidence for a heating immediately before the burst, but it is unclear how it is related to the previously known long-lasting gradual increases in the SXR and microwave fluxes before the flare.

(b) Line broadening and blueshift

Precise measurements of the resonance line profiles of Ca XIX and Fe XXV have led to a discovery of very broad line profiles with a blueshifted subcomponent in the early phase of the flare (Doschek et al. 1980; Antonucci et al. 1982; Tanaka et al. 1982d). The broadest line profiles are generally found at the earliest time of observations, though some cases show a slight increase with time. The maximum width of the Fe XXV resonance line from the Hinotori observations is $54–130\times10^6$ K (average 83×10^6 K) in terms of the ion temperature (T_i). A nonthermal random velocity of 44–170 km s^{-1} is derived, if T_i is assumed to be equal to T_e. The line width decreases monotonically in the later phases approaching a thermal width equal to T_e. It is generally accepted that the large line width represents nonthermal random motions. If one interprets it as thermal broadening (T_i), a long-persisting, large difference between the ion and electron temperatures [T_e (XXVI) and T_e (XXV); figure 8] would contradict a short equilibration time ($\tau_{i\text{-}e}$) between electron and ion for a reasonable density ($\tau_{i\text{-}e}=3$ s for $n_e=10^{11}$ cm^{-3}). However, there remains some possibility that the actual time profile consists of numerous unresolvable impulsive ion heatings

which decay instantaneously. A study of the maximum width in 13 flares shows no systematic limb effect (Tanaka 1986b). On the other hand, flares with greater X-ray source size show smaller width compared to those with compact source size. The impulsive flares show larger width than the gradual-hard flares. The latter show a less remarkable time variation of the width. There is no correlation found between the maximum widths and the maximum electron temperatures. Large line broaending appears to exist also in the Fe XXVI resonance lines (Tanaka 1986b). In two behind-the-limb events, for which the hot thermal component is more conspicuously seen, peculiar Fe XXV profiles having a broader Gaussian wing have been observed (Tanaka 1986b). This may imply the presence of larger nonthermal motion in the hot thermal component.

The blueshift is an excess emission on the shorter wavelength side of the resonance lines. Subtraction of a symmetrical profile obtained by folding the red wing reveals a blueshifted emission hump clearly displaced from the line center. Displacement decreases with time, typically, from 400 km s^{-1} to 250 km s^{-1}, and its equivalent width relative to the stationary component decreases from 20% to 3–5% during the impulsive phase and then almost to zero in the later phase (TZ85). Though the decay curve of the blueshift is similar to that of the line broadening, the former shows a strong limb effect which is not found in the latter. Flares showing the blueshift are limited to those that occurred at a heliocentric angle less than 68° in the Hinotori results (cf. Tanaka et al. 1982d). The limb flares show generally symmetrical profiles, but much smaller blue or red asymmetry are occasionally observed (Tanaka 1986b). The absence of the blueshift near the limb provides a strong basis to interpret it as due to vertical flow presumably along the loops.

Figure 11 shows time profiles of nonthermal line broadening velocity, blueshift, and their correlations with other flare parameters for the best studied case of 1982 June 6 flare (TZ85). The blueshifted profile is most conspicuously seen in the initial phase prior to the main HXR burst. However, the emission measure of the blueshifted subcomponent increases concurrently with a rapid increase in the HXR burst, remains at a maximum ($10^{48.5}$ cm^{-3}) during the peak phase of the burst, and decreases towards the end of the burst. This emission measure history shows best correlation with the electron temperature profile [T_e (XXV)], though it also shows good correlations with the 67–100 keV profile and the light curve of white-light emission. Two emission measures, respectively, of the blueshift and the stationary component of the Fe XXV line are well correlated such that the latter increases following a time integration of the former and reaches maximum at the decreasing epoch of the former. These facts support the idea that the blueshift represents evaporating hot material from the base of the loops as originally suggested by Antonucci et al. (1982). An alternative possibility may be that of rising hot material associated with the prominence eruption. However, this interpretation conflicts with some observations. The blueshifted emission measure shows an increase for a long time (7 min) after the prominence erupts, and shows a persistent (5-min duration) maximum. The SXR contours in a limb flare show no trace of emission (above 10% of the contour peak) at the locations of the rising prominence (Takakura et al. 1987). In addition the SXR images at the rising phase of the blueshifted emission measure in the June 6 event showed a de-

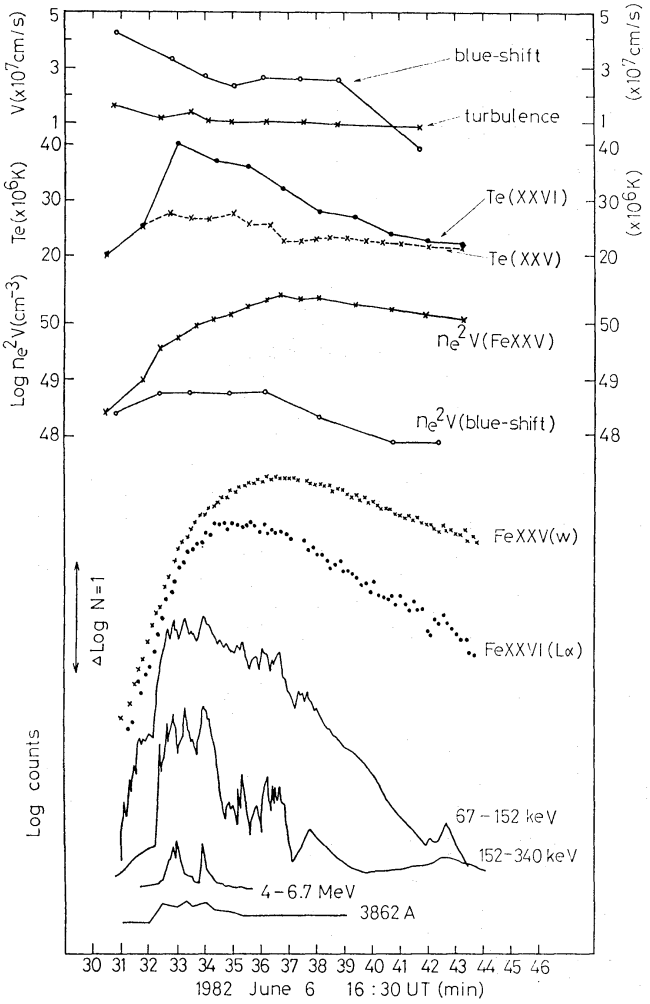

Fig. 11. Time profiles of various plasma parameters and fluxes for the 1982 June 6 flare (X12). From top: blueshift and turbulence velocities of Fe xxv resonance line, electron temperatures from Fe xxvi and Fe xxv spectra, emission measures of stationary and blueshifted components of Fe xxv line, and fluxes of Fe xxv and Fe xxvi resonance lines, HXR at two channels, and 4–6.7 MeV (chiefly nuclear γ lines) and 3862 Å (white light). Reproduced from TZ85.

velopment of double peaks at the footpoint regions embedded in the diffuse extended contours (figure 2d). The prominent peak is concentrated at a dominant optical kernel, and the other less prominent peak is located at the conjugate footpoint to the former and almost coincides with a peak in the HXR image (figure 2c). Presumably the HXR peak would represent the electron-precipitating footpoint and the peak dominated by SXR may represent the footpoint of a high conduction flux which accounts for most of the evaporation.

The initial behavior of the blueshift and broadening may be of interest from a viewpoint of their origins. If the hot flare plasma is provided by the evaporation, an initial line profile will be totally blueshifted and then, a peak will develop at the stationary wavelength. During this transition a doubly peaked profile will be expected as demonstrated by hydrodynamical simulations of a flare loop by Cheng et al. (1984)

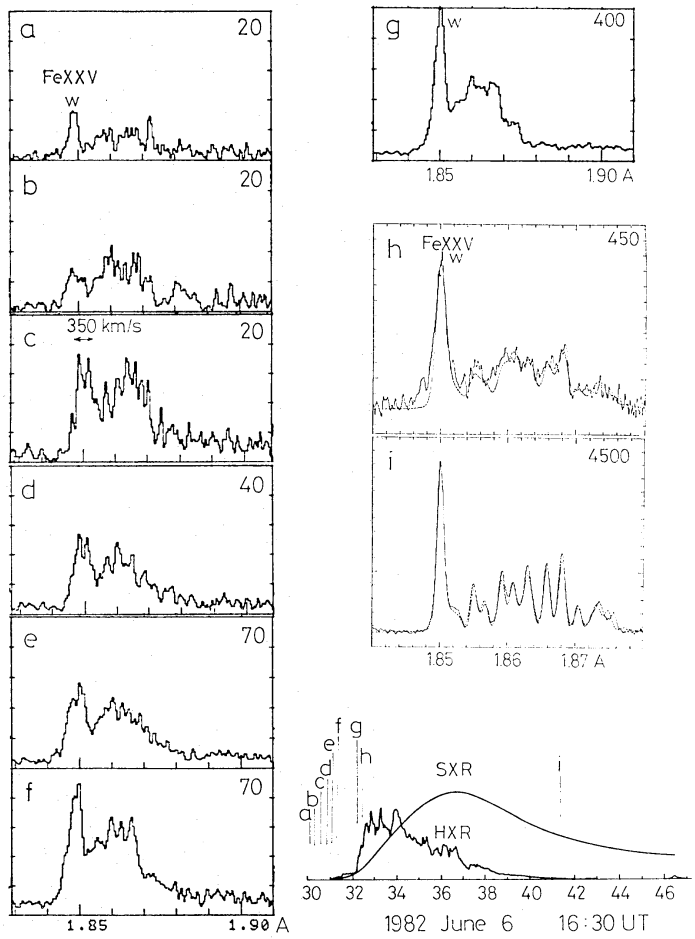

Fig. 12. Time sequence of Fe XXV resonance line (w) profile in the 1982 June 6 flare showing initial development of blueshift and line broadening (see text). (a)–(g) are obtained with the lower-resolution spectrometer, while (h)–(i) are from the higher-resolution spectrometer. Times of (a)–(i) are indicated in the time profiles shown at right bottom. The wavelengths in (a)–(g) are calibrated in reference to the Kα line at 1.94 Å. Theoretical fits to the stationary spectra are given by dash lines in (h) and (i). Count corresponding to full ordinate scale is given in each frame.

and Akita (1985). The Ca-line observation in the 1980 May 21 flare (X1 class) by SMM (Antonucci et al. 1985) shows a symmetrical, broad profile before a high-speed (400 km s^{-1}) blueshifted component appears. It is argued that this initial profile is very slightly (0.8 mÅ or 80 km s^{-1}) shifted blueward indicating a slow upward motion of the entire SXR source. On the other hand, the 1982 June 6 flare (X12 class) from Hinotori shows a different behavior for the initial growth of the Fe XXV resonance line which was detected only in the higher sensitivity spectrometer with lower resolution. As shown in figure 12, the earliest profile is singly peaked and displaced blueward by $2\text{–}3\times10^2$ km s^{-1}. It broadens in 10 s becoming doubly peaked with a peak separation of 350 km s^{-1}, and after 40 s the peak on the blue side shrinks to present profiles with a small blue excess such as would normally be observed in the higher-resolution spectra (figure 12h). Fine structures in the line profile change rapidly in 10 s suggesting the broadening is due to discrete multivelocity structures. Note that this development was observed in the very early phase 2 min prior to the im-

pulsive burst, though a slow, gradual increase in the low-energy HXR channels had started together with faint brightening in Hα. Such early behavior has been detected because of its very large SXR flux. This important result, although of marginal statistical significance and at the limit of spectrometer wavelength resolution, nevertheless indicates that a very large broadening at the initial phase was resolved into two separate peaks. This could imply a causal relationship between the broadening and the blueshift. It should be noted that recent SMM BCS results show similar observations indicating discrete short-lived emission features at the resonance lines of Fe XXV and Ca XIX during the impulsive phase of two flares (Bentley et al. 1986; Doyle and Bentley 1986).

In this way, due to the limited number of good observations on the early history of the line broadening, the origin of the broadening remains controversial. It may result from the convective velocities driven by evaporation. A large velocity dispersion would be expected from the velocity gradient along a loop (cf. Nagai 1980) or from evaporations in numerous unresolved loops with different inclinations to the surface. The presence of discrete narrow emission features at the very early phase as cited above suggests that the broadening at this stage may be resolved into multiple mass ejections which may occur associated with individual electron-beam impacts or with spraylike ejections (cf. Doyle and Bentley 1986). Alternatively it may manifest a turbulence intrinsically related to the primary magnetic field instabilities. Antonucci et al. (1986) considered the outflow motions from reconnection sites scattered along the loop. We may recall that turbulent motion of 50–100 km s^{-1} is observed in the Hα filament-during its activation phase immediately before the flare (Zirin and Tanaka 1973). Also in the filament disruptions (Roy and Tang 1975) preceding the the flare turbulent motions occur in the many features comprising the filament. Such turbulent motions, causing dynamical interactions among the magnetic lines of force, may possibly be related to the energy conversion mechanisms through tearing mode or current-tube coalescence instabilities, and may give rise to the high-temperature turbulence observed in the SXR.

(c) Kα emission and line polarization

The Fe II Kα lines at 1.930 Å and 1.936 Å are emitted from the photospheric neutral iron when a K-shell electron is removed either by fluorescence due to the SXR irradiation or by collisional impact of the electron beams. It has long been anticipated that direct evidence for the electron beam could be provided by a detection of the transient iron Kα emission (Phillips and Neupert 1973). For the long-lasting weak Kα emission seen in all flares, the fluorescence origin has been established (Parmar et al. 1984). Transient Kα emissions that are exceptionally intense in the early impulsive phases have been reported from Tansei IV (Tanaka 1980) and Hinotori (Tanaka et al. 1983). These emissions were at first interpreted as providing evidence for the collision-impact origin (Tanaka et al. 1983) but later analyses (Tanaka et al. 1984) combined with observations of the SXR continuum spectra revealed that it could be explained by the irradiation of the photosphere by an impulsively varying X-rays of a power-law spectrum which extends to a threshold (7 keV) of K-shell ionization. The efficiency of the Kα due to the electron collision impact is shown to be lower than the fluorescence Kα due to the irradiance of the power law X-ray which is radiated

by thick-target mechanism by the same electron beams (Tanaka et al. 1984). Thus, direct collision by nonthermal electrons seems not to be required to explain the transient Fe Kα emission.

Another direct diagnosis for the collimated electron beam may be obtained from detection of X-ray line polarization (Haug 1979). Early observations from the Intercosmos (Krutov et al. 1981) suggested a strong polarization. Precise measurements of the line polarization, using the rotating Bragg spectrometers on Hinotori, demonstrated low polarization ($<4\%$) for most phases of flares (Akita et al. 1983; Akita 1985). However, one candidate for the occurrence of impulsive polarization of about 10% is reported associated with a very sharp HXR spike in the 1981 April 4 flare (Tanaka et al. 1982c; Akita 1985). The result is compatible with a nonthermal population which was about 1% of the thermal population according to Shlyaptseva et al.'s (1981) model, but the duration is too short (20 s) to derive convincing result from this spectrometer with a time resolution of 10 s. At the instant of the peak of this HXR spike a very strong transient emission was observed at 1.792 Å (dielectronic satellite from Fe XXVI) without accompanying Lα lines (Tanaka et al. 1982a, p. 254; Tanaka et al. 1982b). This peculiar emission provides a unique candidate for the nonthermal excitation of the SXR line. In conclusion, the population of highly collimated nonthermal electron beams seems to be mostly negligible in low-energy region (5–10 keV). This is consistent with the low degree of polarization (upper limits between 2.5 and 12.7%) found from the continuum measurement in the energy range from 5 to 20 keV by Tramiel et al. (1984).

5.2. *Properties of the Hot Thermal (Superhot) Source*

The spectroscopic evidence for a large hot thermal component of $T_e > 3\times10^7$ K in a substantial number of flares confirms thermal HXR emission in the region of 15–40 keV. Then, morphological properties of the hot thermal component can be derived from this HXR emission. The HXR images give a compact ($<15''$) roundish morphology. The type A flares show particularly compact size ($<10''$) and low height (<6000 km) (Tsuneta et al. 1984a). The source shows an evolution characterized by upward source shift. For a limb flare (1981 October 7) whose time profile is given in figure 8a, the heights of the centroid of the hot thermal source and the top of the Hα loops are plotted against time in figure 13. The centroid increased from 10^4 km to 1.5×10^4 km during 7 min (Ohki et al. 1983). The Hα loop prominence system appeared first at 23:03 UT at 7×10^7 km, at the same location as the hot thermal source with a lag of 10 min from the HXR source and successively at higher altitudes tracing the HXR sources with a similar upward velocity. It implies that the hot thermal source cools rapidly to 10^4 K and appears in the form of Hα loops. A cooling time of 10 min is suggestive of high density over 10^{11} cm^{-3} for cooling either by conduction or by radiation (Feldman et al. 1982b). The apparent upward motions could reasonably be attributed to the sequential formations of different loops at successively higher altitudes. Similar evolution is observed for the SXR thermal component in an impulsive flare which showed no hot thermal component. As shown in figure 5, this source is initially located very close ($<10''$) to the two shallow ribbons (due to the projection). In a 5-min interval, still during the impulsive phase, the source is

displaced by 20″ from the ribbons and moves outside the limb. Successive displacement occurs with a velocity of 40 km s^{-1}. The SXR images from the Skylab also give similar evolution in the later flare phase (Moore et al. 1980). Seely and Feldman (1984) derived, based on the Bragg angle measurement, that the centroid of the Ca XIX emission region moves to a higher altitude with 20–40 km s^{-1} and reaches $3–4\times10^4$ km in 20–30 min.

Morphological and timing relationships between the formation of these X-ray sources and the prominence eruption are suggestive. In figure 5 the SXR and HXR sources appeared during the activated phase of the prominence before rapid rising motion started. They are not located at the major part of the prominence but beneath it, near one leg of the prominence. The major part of the prominence ascended during the burst with a velocity of 200 km s^{-1}. In the 1981 October 7 flare the hot thermal source also appeared at one leg of the prominence synchronous with its eruption (figure 13). This part of the prominence splashed away and the other leg stretched during the prominence ascent. The ascending velocity (200 km s^{-1}) of the prominence far exceeds the upward source motion (10–15 km s^{-1}). From these results a morphological model as shown in figure 14 may be suggested.

One property that may distinguish the flares with hot thermal component from those without would be their high density. The mean density derived from the HXR source size and Fe XXVI emission measure exceeds 10^{11} cm^{-3} (Tanaka et al. 1982d;

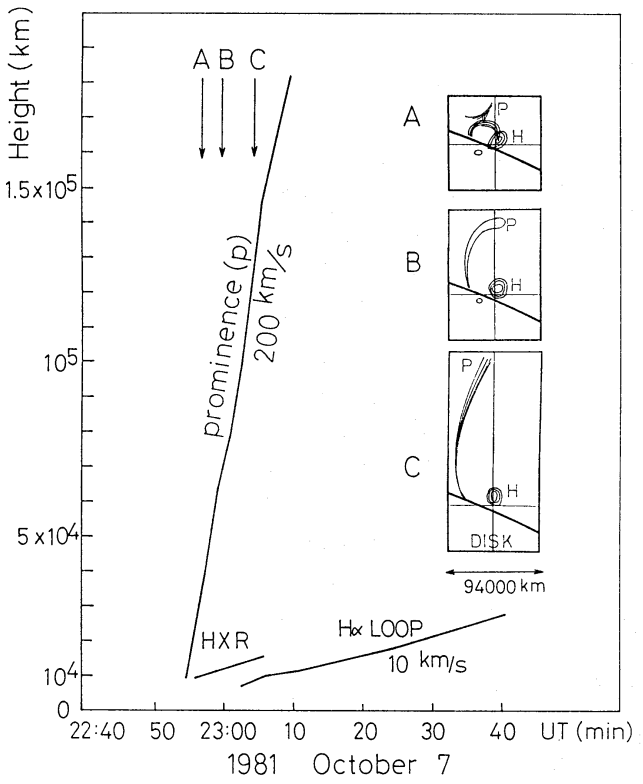

Fig. 13. Height loci of centroid of the hot thermal source in HXR images, Hα loop top, and ascending prominence for the 1981 October 7 flare (cf. figure 8a). At right are shown HXR contours (H: from Ohki et al. 1983) and erupting prominence (P: from Big Bear Observatory) at three phases (A, B, and C).

Tsuneta et al. 1984a; Tanaka 1986a). On the other hand, the mean density of the SXR thermal source in the absence of the hot thermal source is below 10^{11} cm^{-3}, typically 3–5$\times 10^{10}$ cm^{-3}. Densities exceeding 10^{12} cm^{-3} are suggested from the very fast decay of some SXR flares (Feldman et al. 1982b), and also, for cooled loops, from the presence of bright He I D3 loops seen as emission against background (TZ85) and from the H I Balmer line widths. The fact that Hα loops are much brighter and appear much earlier in flares with enhanced hot thermal components than in flares without a hot thermal component (Tanaka 1986b) demonstrates higher density in the loops rich in the hot thermal component. High density and temperature in this component require magnetic field strength higher than 330 G to confine this plasma (Tsuneta et al. 1984a).

Another characteristic of those flares rich in the hot thermal component may be suppression of the impulsive component. The 1981 April 2 flare (canonical type A flare) shows a very smooth rise and fall at 17–40 keV (figure 1d). Some spikes that are clearly visible above 40 keV are totally missing in this energy range. By a power-law extrapolation from the spectrum above 40 keV one of the spikes should have a count of 6300 cps in 17–40 keV and should be visible superposed on the smooth profile which shows a count of 12000 cps at this time. Thus the missing spike is not hidden by the dominant hot thermal component, but indicates a real shift of the low-energy threshold of the impulsive component to a higher energy above 40 keV. The cutoff energy in the impulsive flares usually lies below 20 keV as mentioned earlier. Secondly, flares which are more effective in producing the hot thermal component tend to have softer spectra for $E>40$ keV to which the hot thermal component contributes little. Figure 9c shows a plot of this spectral index (γ) versus peak intensity ratio of the Fe XXVI to Fe XXV lines for various flares. The latter denotes relative population of the H-like ion to that of He-like ion, and hence the relative significance of the hot thermal component. Two clusters in this diagram represent "high temperature" flares and "low temperature" flares denoted in figure 9a, respectively. A positive correlation is evidently found, i.e., flares with inefficient generation of the hot thermal component show systematically smaller γ. In particular, the flares with the hardest spectrum ($\gamma<3.5$) belong to the "low temperature" class. This correlation is consistent with the fact that the hot thermal component is generally insignificant in the gradual-hard flares which show systematically harder spectra compared to the impulsive flares. The hot thermal flare is also known as emitting a very weak microwave flux (Tsuneta et al. 1984a). With the strong magnetic fields suggested in this type of flare, this implies a suppression of the particle acceleration. These tendencies may suggest that effective heating and effective acceleration are complementary in individual flares. Further the two characteristics, i.e., effective heating and high density in the hot thermal flare may well be related intrinsically.

The very high temperature and compact source size of the hot thermal source may pose problems for energetics and plasma confinement. High efficiency of conduction might inhibit a localization of the high-temperature region near the loop top and also require too much energy to maintain the source. The heat conduction loss estimated by classical theory amounts to 2×10^{28} erg s^{-1} (Tsuneta et al. 1984a) and 7×10^{29} erg s^{-1} (TZ85), respectively, for the X1 class and X12 class flares. Since the

total thermal energy at the peak is respectively 2×10^{30} erg and 2.6×10^{31} erg in these flares, the cooling time becomes about 100 s and 40 s respectively. These are much shorter than the lifetime (about 500 s) of the hot thermal source, but by considering that the source is successively formed at higher levels as shown before, the lifetime at one height is much shorter and consistent with these cooling times. In addition, the actual conduction loss would be lowered, since the classical theory may be invalid due to the small source size comparable to the mean free path (Duijveman 1983) and also if the relevant filling factor for cross-sectional area of the loops is taken into account. The confinement problem also seems to be explained in terms of a steady conduction model. Under the classical conduction theory Takakura (1984) proposed two steady-state models. In the high-density case ($n_s=10^{12}$ cm^{-3}) the peak temperature (T_s) of less than 5×10^7 K is maintained by constant energy generation at the loop summit and heat loss by conduction to the legs of the loop from which the energy is radiated. Pressure balance is assumed along the loop. This leads to a scaling law: $n_s=10^6T_s^2/L_s$ (L_s is a half loop length), similar to the one derived for a stationary coronal loop by Rosner et al. (1978). By this model the loop brightness at 15 keV X-ray falls to 1/3 of the peak brightness at the summit within a half of the loop length. Therefore, a high concentration of the X-ray intensity near the loop summit is consistent with this model. The other case investigated is a high-temperature model with T_s upto 3×10^8 K and $n_s=10^{11}$ cm^{-3}. The radiation loss from the loop is negligible in this case so that the heat flux is nearly conserved down to the footpoints. The resultant temperature gradient is smaller and the X-ray brightness distribution is much more extended along the loop.

5.3. *Origin of the Hot Plasmas*

For the origin of the hot flare plasmas chromospheric evaporation has been postulated for more than a decade (Neupert 1968; Hirayama 1974). The results from Hinotori as well as from other observations have provided some evidence for the evaporative process, but also seem to indicate that in-situ heating occurs in the corona. Here I discuss indications for both processes and their mechanisms. The evaporation hypothesis may be supported by the following results:

(1) The presence of upflows in the early flare phase as evidenced by the blueshift (300–400 km s^{-1}) of the X-ray lines in the disk flares.

(2) The emission measure history of the blueshifted component matches an increase in the emission measure of the stationary component [Fe XXV observation by TZ85; Ca XIX observation by Antonucci and Dennis (1983)].

(3) The total amount of the hot plasma derived from Fe XXV emission increases from the beginning till the vanishing phase of the blueshift [in the X12 flare $N=3.5\times10^{38}$ to $N=2.5\times10^{39}$ (TZ85)].

(4) The mean electron density of the hot plasma increases monotonically towards later phases [in the X12 flare $n_e=2.5\times10^{10}$ cm^{-3} to $n_e=2\times10^{11}$ cm^{-3} (TZ85)].

(5) The temporal increase in the total number N derived from the Fe XXV emission is explained by the mass input estimated from the blueshift emission and the footpoint area of optical kernel when due account is taken of a filling factor in the vertical direction along the loop [rising materials occupy geometrically 1/6 to 1/12

oft he loops (TZ85)].

(6) The number of atoms evaporated from the chromosphere as derived from the Hα profiles agrees with the total number above 2×10^6 K (Acton et al. 1982).

(7) The momentum transported by the upflowing SXR (Ca XIX) plasma equals that of the downflowing Hα material (Canfield et al. 1987).

(8) The temporal increase in the thermal energy of the hot plasma is explained by the enthalpy and kinetic energy input from the blueshifted plasma (Antonucci et al. 1982; TZ85).

(9) The early SXR images show intensity peaks at footpoint places (Antonucci et al. 1985a; TZ85; figure 2d).

(10) The initial development in the Fe XXV line profile indicates, though marginally, an evolution from blueshifted single peak to doubly peaked profiles (figure 12).

(11) Hiei and Widing (1979) observed a progressive brightening from the footpoint to the top of a loop in a Skylab flare.

A number of numerical simulations have been performed for a hydrodynamic response of the flare atmosphere to heating due to electrons or conduction and have demonstrated the effectiveness of the chromospheric ablation and subsequent expansion of heated plasmas into a loop. As summarized by Fisher et al. (1984), the evaporation driven by an electron beam which accounts for high coronal plasma temperatures ($>10^7$ K) is limited to cases with high input flux above 3×10^{10} erg s^{-1} cm^{-2} and occurs mostly explosively with an expansion velocity of about 1000 km s^{-1}. In contrast the conduction-driven evaporation leads to a slow expansion with $v=400$ km s^{-1} consistent with the observed velocities and temperatures. The input energy fluxes compatible with these calculations range from 3×10^9 to 10^{10} erg s^{-1} cm^{-2}. Akita (1985) investigated the effects of initial loop density in the beam-driven cases, and showed that under a high (3×10^{10} cm^{-3}) initial loop density consistent with the observations the electron beam model causes a slow expansion. In this case a major portion of the beam energy (10^{11} erg s^{-1} cm^{-2}) is deposited in the corona due to the dissipation of low energy electrons ($E>15$ keV) and conducted downwards resulting in thermally-driven evaporation. Thus the conduction seems to play an essential role in the evaporation even if the beam exists. The conduction-driven evaporation process is supported by observations indicating the presence of high temperature ($>10^7$ K) and conspicous blueshift before the impulsive HXR burst (cf. figures 8b, 11, 12). Acton et al. (1982) suggested based on the Hα, SXR, and HXR images that chromospheric evaporation is driven by both mechanisms. Actually there is evidence for electron heating of the deeper chromosphere, namely the detection of very broad Hα profiles (Acton et al. 1982) and white-light emissions. But, because such heating appears in a very limited portion of the flare area, the evaporation directly driven by the electrons would have a minor contribution to the total mass budget.

We now argue for the coronal in-situ heating. The results suggesting this are as follows:

(1) The loop top region is bright from the beginning of the flare as observed in the thermal HXR burst contributed by the hot thermal component. Especially in the case of behind-the-limb events, the centroids of the thermal sources are located above the limb from very initial phase (Takakura et al. 1983c; Tsuneta et al. 1984a;

Tanaka 1986b).

(2) The SXR images in the initial phase of June 6 flare (TZ85) are more extended than the HXR source and optical footpoint region. The SXR source, when projected close to the limb, shows contours always peaked above the two ribbons or above the limb including the cases of progressive loop activations at higher levels. The Fe XXIV image obtained in the Skylab EUV spectroheliogram gives an emission confined near the loop top from the early stage of the flare (Widing and Dere 1977).

(3) The mean densities of the SXR sources and thermal HXR sources are both high, being about 3×10^{10} cm^{-3} and $>10^{11}$ cm^{-3} respectively from the flare beginning. High densities of over 10^{11} cm^{-3} are derived from the line intensity ratios for all phases of the flares observed by the Skylab (Dere et al. 1979).

(4) T_e (XXVI) is high ($>3\times10^7$ K) and deviates substantially from T_e (XXV) from the flare start in behind-the-limb events indicating the generation of a hot thermal component of $T_e>3\times10^7$ K, preferentially, at higher altitude than the SXR thermal component of $T_e<3\times10^7$ K (Tanaka 1986b).

In fact the actual situation may be hybrid. The higher temperature plasmas, in particular, those with $T_e>3\times10^7$ K appear to be generated at the loop top from the flare start. The dominance of this component in the maximum or postmaximum phases does not necessarily imply a second-stage heating of previously evaporated material, since the loops at this stage are located at higher levels than are the early stage loops. As suggested the heating would occur successively in higher loops. In individual loops a generation of the higher temperature plasma at the loop top would be followed by an evaporative supply of the lower temperature plasmas ($<2\times10^7$ K), and, due to rapid cooling of the former, the two kinds of plasmas of different origin would be mixed in a loop without a sharp boundary. As this sequence would occur in successively higher loops, at any one instant the high-temperature plasmas would be seen predominantly at higher locations, while the lower-temperature plasmas would occupy lower loops. As far as abundances are concerned, the low-temperature plasmas would dominate over the higher-temperature plasma and explain the emission measure increase in the post-T_e maximum. A crucial feature of this scenario may be how to explain the fact of high coronal density from the flare start. The high density may possibly be caused by preliminary evaporation due to the preburst coronal heating (section 5.1a), plasma compression during the heating process, and density increase associated with the preflare density increase in the filament which is manifested in the thickening and darkening of the filament (Tanaka 1976).

As for the mechanism of the in-situ heating the electron-beam heating would be a strong candidate. The thick-target nonthermal model would inevitably produce large energy deposits in the corona and chromosphere. As discussed before, a major deposit would appear in the corona due to the dissipation of the low-energy electrons. It is shown observationally that the total thermal energy derived from the Fe XXV emissions agrees fairly well with this energy deposition above certain cutoff energy, which varies from 30 keV for the impulsive flare to 50 keV for the hot thermal flare (Tanaka et al. 1983). A higher cutoff energy for the latter is suggested in section 5.2. For some impulsive flares a temporal increase of the SXR thermal energy is nicely fitted by the electron injection curve corrected for coolings with a threshold of 25 keV

(Antonucci et al. 1984b; also for the 1982 January 22 flare, K. Tanaka and N. Nitta, private communication). One should note that these agreements do not necessarily argue for the evaporation due to the electrons, since the electrons with this cutoff energy may be dissipated in the corona and the deposited energy is considered to be transferred to the evaporated plasmas via conduction. There are some controversial cases for this energy budget, however. In a small flare (M3.4 class) which presented a single power-law down to 7 keV, the total energy deposit above 7 keV amounted to 1.5×10^{32} erg, which is two orders of magnitudes larger than the thermal energy (Tanaka et al. 1984). In the big X12 flare the electron energy above 20 keV is estimated to exceed 10^{33} erg, whereas the total thermal energy is 2.6×10^{31} erg and the magnetic energy stored due to the sunspot motion is 4×10^{32} erg (TZ85). In this case, the X-ray flux below 40 keV is saturated but probably the cutoff energy would be higher than 40 keV as the flare is characterized by a pronounced hot thermal component, which would resolve the discrepancy. With the lack of information on the precise value of the cutoff energy this kind of comparison would not lead to further convincing argument for the beam heating. One aspect supporting the electron heating may be an observed fast response of the SXR emission to a sharp HXR spike as shown in figure 1a (Tanaka et al. 1982c). Numerical modeling by Akita (1985) could reproduce the observed SXR time profile for a given electron beam input, which is postulated from this HXR spike, in a situation of high coronal density (3×10^{10} cm^{-3}). In lower densities the SXR profile becomes double-peaked; one peak is associated with the in-situ heating due to the electrons and the second major peak is due to the compression of evaporating materials at the loop top. This case is not in accord with the observation.

There are some observations that may appear to contradict the beam heating. The distinct disagreement of the rapidly varying HXR source structure with the stationary SXR source such as shown in figure 3 implies that dissipation of the electrons occur at different places from the SXR emitting loops in the impulsive phase of some flares. Some SXR time profiles show no response to the HXR peak such as is often witnessed in the gradual-hard flare (figures 1e, 6b). These cases suggest that at least some part of the electron energy is deposited at places different from the high-density loops without contributing the SXR emissions (cf. Feldman et al. 1982a). The hot thermal component is enhanced in some flares during a gradual phase in which the impulsive burst is negligibly small (figure 8a) and in others during the impulsive phase (figure 11). The latter may be compatible with the beam heating in the loop as suggested by Lin et al. (1981), but the former would exclude this possibility.

Probably in actual flares several (in-situ) heating mechanisms and evaporation process may work simultaneously and their contributions may differ depending on the ambient conditions. Among the candidate mechanisms besides the electron-beam heating would be ion heating, Joule heating, turbulence, compression (contraction), shock heating, and radio maser mechanism (Melrose and Dulk 1984). It is premature to specify the most efficient mechanism. One interesting point that needs to be explained may be the aforementioned (section 5.2) inverse correlation between the efficiencies of generation of the hot thermal component and the electron accelerations. The relative efficiency of the heating to the acceleration seems to increase at higher

ambient density (section 5.2). Under the assumption that heating and acceleration take place at the same location this suggests that partitioning of the released energy into the two modes may be controlled by the density at the energy conversion site. Tsuneta (1985) has shown that the Joule heating satisfies this condition.

6. Suggested Flare Scenario

A basic magnetic configuration that plays an essential role in the flare occurrence is magnetic shear (cf. Zirin and Tanaka 1973; Tanaka and Nakagawa 1973). The sheared fields contain highly concentrated field-aligned current which would be responsible for the micro- and macro-scopic instabilities in the flare. As may be inferred from the fact that flare-rich sunspot groups of δ-configuration show high shear and inverted polarity from their birth and continuous changes of magnetic flux during their evolutions characterized by the shear motion, the magnetic shear may be considered to be provided principally from below the surface by the emergence of flux. The birth and complex evolution of the δ-group are explained phenomenologically as a continuous emerging process of tightly-twisted magnetic tubes (knot) from below the surface (Tanaka 1986c), and the flare energy is explained to be supplied associated with the emergence of a twist (Tanaka et al. 1980). Although the flux tube may undergo various modifications, after the emergence, due to interactions with preexisting fields and subsurface flows, the flare energy may be contained basically in the proper shape of the flux tube stressed during its formation in the convection zone subject to various distorting forces due to convections, and released after its emergence to the outer layer where the excess current becomes unstable because of the low value of β in the plasma. Thus observed varieties in the active region morphology and the flares would be a consequence of the chaos in forming and stressing the magnetic tube in the convection zone.

From this point of view we may attribute the great variety of flares revealed by Hinotori to the varied morphology of magnetic stress and the different time sequences of energy release. In particular, great differences in the time scale and manner of generating high-energy particles between the impulsive and gradual-hard flares seem to result from different energy release sequences in different magnetic field assemblies. The impulsive flare (type B) generally occurs in a region of high magnetic shear represented by a low-lying active region filament. In this configuration a bundle of the magnetic lines of force turns sharply above their photospheric footpoints to the horizontal direction and runs parallel to the inversion line merging together the nearby active region fields which later become flare loops (figure 14a). The flare is preceded by an activation of the filament and subsequent eruption which is presumably caused by MHD-type instabilities associated with a new flux emergence under the filament, or with an increase of axial current in the filament (kink), or with a wave propagation from below the surface (cf. Uchida and Shibata 1984). The filament eruption would disrupt dynamically those magnetic fields folded with or overlying the filament, and, through reconnections or expansions, gives rise to impulsive energy releases in these fields successively (figure 14b). A chain of HXR spikes of random amplitude would represent such a sequence of the impulsive energy releases spreading to a number of

field lines which originally contain high current. Fast (1–10 s), multiple energy releases in complexly sheared low-lying fields have been manifested by the impulsive Hα brightenings at several footpoints distributed on the immediate side of an erupted filament as well as by the low, extended HXR source structure. Energy releases in disordered magnetic fields, which may originally be entangled with the erupted filament, may be inferred from the nonsymmetric irregular distributions of initial optical footpoints along the inversion line as noted in section 3. The impulsive nature of these energy releases may be due to the rapid growth of resistive instabilities in individual field lines, which seems to be a natural consequence of the high current concentration in low-lying sheared fileds. Also a fast energy-release sequence would result from a rapid MHD disruption of the preflare magnetic configuration manifested by the prominence eruption.

In contrast, the gradual-hard flare starts slowly without filament eruption in a region characterized by large spots and extended plages with a faint undeveloped filament. The Hα footpoints are distantly separated from the inversion line from the start. This, together with the high, extended source structure in HXR, suggests flare occurrence in large field lines extending to high ($>$40000 km) altitude and having a bottle-shaped configuration. The lack or weakness of the impulsive phase may be related to the absence of the filament eruption. Without the explosive trigger mechanism symbolized by this eruption the energy releases may be initiated at high fields and proceed slowly but progressively to higher fields. This flare progression to outer and higher fields occurs in discrete steps from one local assembly of the field lines to the next with a time scale of a few minutes as can be seen from the two-ribbon development (figure 6). The HXR source shows gradual small shifts associated with this flare development but mostly remains stationary under the present low resolution. Particles are not impulsively accelerated in a single magnetic loop as in the impulsive flare, but appear to be progressively accelerated as they drift to adjacent (higher) loops as described in section 4. They may be trapped in the bottle-shaped fileds due to mirroring, and move to different field lines by curvature drift or nonuniform B drift in the course of acceleration. The slowness in the development and energy release may be principally related to the low current density and lack of the violent trigger mechanism. The former is inferred from the large-scale magnetic configuration with weak shear as shown by the reasonable fit with the potential fields (Sakurai 1985). In such a situation, the growth rate of the resistive instabilities would be small making the energy release less impulsive. These two patterns of energy release may, more or less, coexist in many flares. In fact, most of the impulsive flares show, in later phases, an evolution similar to that in the gradual-hard flares, i.e., a progressive separation of two ribbons and X-ray source movement. However, the geometrical extension involved is smaller in the former.

In summary, it is suggested that the flare impulsiveness is determined by the degree of current concentration in individual lines of force (i.e., degree of the magnetic shear), while the pattern of flare development is established by the spatial distribution or form of the magnetic shear. These may be the principal factors that distinguish the impulsive flare from the gradual-hard flare. In addition the ambient density may be another key factor that discriminates the hot thermal flare (type A) from others.

The circumstantial evidence suggests that the energy release in conditions of high ambient density leads to efficient heating, especially for generation of the plasmas of $T>3\times10^7$ K but less effective acceleration. Various heating mechanisms as well as the acceleration mechanisms would fit this situation. In order to justify and find specific mechanisms we will need to identify the acceleration site as related to the heating site. The high ambient density may be due to the emergence of a compact tightly twisted magnetic configuration whose low height and high fields are able to contain a large amount of mass after the flux emergence.

Although the differences in the magnetic configuration and scale may cause flare developments with different time scales and patterns, basic flare evolution in most flares would be similar in the sense that multiple discrete field lines are progressively involved in the flare. The Kopp–Pneuman-type model (Hirayama 1974; Kopp and Pneuman 1976) explains the successive formation of higher loops by progressive reconnections of the field lines which initially overlie the filament and open up due to the rising motion of the filament. The long-lasting (>10 h) formation of the post-flare loops may strongly support this type of model as argued by de Jager and Švestka (1985). However, it is unclear whether the following points revealed in this paper can be explained by this model. The initial energy release appears to take place at one leg of the filament before it is lifted. The rising velocity of the prominence much exceeds the velocity of the upward movement of the X-ray source or the reconnected point in this model. Expansions of two ribbons are irregular, and particularly their initial development does not suggest a symmetrical arcade of loops but a complex ensemble of intricate field lines. Some footpoints appear at places closer to the inversion line than the preceding ones (figure 2b). The gradual-hard flares show progressive formation of higher loops without being accompanied by filament eruption. Progressive separation of two ribbons is restricted to a local region along the inversion line with other places showing slower separation or even no separation at all. In the impulsive flare initial energy releases seem to take place in the low-lying, horizontal fields located, with high shear, under the filament. The gradual-hard flare (at least the May 8 event) occurs in the loops anchored at the two umbrae in some phase. It is questionable how such strong fields can be opened.

The flare magnetic configuration proposed in figure 14 may explain some of the points mentioned above, though it may be difficult to explain the long-lasting loop formations. In this model the preflare sheared non-force free fields which are confined to the filament channel are unfolded by the filament eruption, and expand in succession relaxing to force-free or potential fields. During each eruptive process the excess current included in the field line may be dissipated. Expansions in an irregular sequence may result from successive unfoldings of a complexly sheared configuration. The fields are postulated not to be opened, though reconnections might occur between those fields originally folded in the filament channel. Without the association of the filament eruption in gradual-hard flares, the successive field expansions may also be induced by some propagating trigger agent; the preflare field assembly may become unstable due to a flux emergence or wave propagation from below and collapse dynamically from low to high altitudes. Alternatively a snap-back of lower field lines may force the snap-back for higher fields in succession (Tanaka 1978).

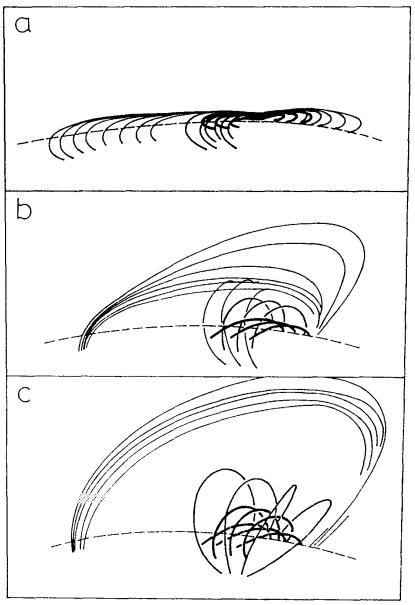

Fig. 14. A proposed model for the magnetic morphology in the impulsive flare. (a) Preflare configuration showing complexly sheared low-lying fields folded in the filament fields. (b) A filament eruption disrupts and unfold the sheared fields confined near one leg of the filament, successively, from lower to higher fields. (c) Postflare loops in vertically sheared configuration with lower and higher loops being represented respectively by the force-free and potential fields (cf. figures 5 and 13).

Accelerations may take place during the elementary eruptive process by the $V\times B$ mechanism (J. Sakai 1986, private communication; cf. Sugihara and Midzno 1979), or it may take place at the intersectin gpoint of two dynamically interacting field lines by a reconncetion mode of the current loop coalescence (Tajima et al. 1982), which is found to be very explosive and yields efficient bulk energization and acceleration of electrons and protons.

Finally we summarize the energy transfer in a flaring loop. The following view may be derived for the impulsive flare from the Hinotori results with incorporation of other results. Due to the energy conversion from the magnetic fields heating will result at the loop top generating high temperature plasma (especially the hot thermal component of $T>3\times10^7$ K), and the heat is conducted down to the transition region causing evaporation. The electron and ion accelerations may take place impulsively at the loop top (reconnected site) or at the intersecting points of two loops or in the transiently expanding magnetic field. The low-energy electrons (e.g., 5–25 keV) are predominantly dissipated in the corona producing the coronal thick-target HXR emissions from above the footpoints. The dissipated energy, which constitutes the major flare energy input in most cases, is also conducted downward to enhance the evaporation. Evaporation ultimately supplies the dominant portion of the hot flare plasma above 2×10^6 K, which will be mixed with the higher temperature plasma produced earlier at the loop top. This energy release and transfer would occur sequentially in many loops, thus overlapping various phases of the energy transport in different loops. Although the above view would not contradict the thick-target electron beam model, the presence of highly collimated beams in the low-energy range

may be doubtful. The immediate damping of these electrons in the corona would make heat conduction the major means of energy transport to the chromosphere. Most of the Hα emission would result from the conductive supply. Collimated electron beams that can penetrate to the footpoints are limited to those of high energies, presumably $E>50$ keV. These electrons will excite the upper chromosphere and produce impulsive brightenings in Hα and other visible and UV bands. In particular the electrons in the region of 100 keV seem to be the principal contributor to the white-light emission as evidenced by temporal and energetic correlations (cf. TZ85). They can reach the level of a column density equal to 10^{21} cm^{-2}, i.e., the low chromosphere, and thus explain the emission from H I Balmer continuum. The white light emission which originates in much deeper layers also appears to exist (cf. Hiei 1982), but its excitation mechanism is still unknown. High-energy protons, ions, and neutrons are also produced impulsively together with the electrons. The ions penetrate to the high-density region with $n_e>10^{13}$ cm^{-3} before emitting γ-ray lines by the thick-target mechanism. The neutrons would penetrate to deeper layers ($n_e=10^{14}$–10^{15} cm^{-3}) than the charged particles as is evident from strong attenuation of the neutron-capture line at 2.22 MeV at the limb compared to the nuclear deexcitation line (4.4 MeV; Yoshimori 1985). The deka-MeV continuum emission is remarkably concentrated around the limb (Rieger et al. 1983) and this fact implies that the emitting particles are traveling normal to the sun's center (Kundu and Woodgate 1986).

In the gradual-hard flare the hot thermal component may not be so efficiently produced, since the source location is high and hence the initial density is relatively low. The low,energy electrons may be dissipated high in the corona due to the large path length. The high source would also reduce the conduction compared to the flares occurring at lower levels and result in a weaker evaporation. The large SXR emission measure may be due simply to the large volume involved. The particle acceleration to the MeV range would occur progressively as particles drift to different, adjacent lines of force and precipitation to the footpoints would be suppressed because of a mirroring effect in the bottle-shaped magnetic fields, which characterize the configuration in this type of flare. Probably a substantial number of the impulsive flares may undergo an evolution of the mode of energy release and transfer, similar to those of the gradual-hard flare, as the flare energy release progressively shifts to higher magnetic fields.

The Hinotori project was conducted by the Institute of Space and Astronautical Science (Project Manager, Professor Y. Tanaka). The author would like to thank Professor T. Takakura and Drs. N. Nitta, T. Watanabe, S. Tsuneta, and K. Ohki for providing preliminary or unpublished results, and Professor H. Zirin for providing optical data from the Big Bear Observatory.

References

Acton, L. W., Canfield, R. C., Gunkler, T. A., Hudson, H. S., Kiplinger, A. L., and Leibacher, J. W. 1982, *Astrophys. J.*, **263**, 409.

Akita, K. 1985, Ph. D. Thesis, University of Tokyo.

Akita, K., Tanaka, K., and Watanabe, T. 1982, in *Hinotori Symposium on Solar Flares* (Institute of Space and Astronautical Science, Tokyo), p. 58.
Akita, K., Tanaka, K., and Watanabe, T. 1983, *Solar Phys.*, **86**, 101.
Antonucci, E., and Dennis, B. R. 1983, *Solar Phys.*, **86**, 67.
Antonucci, E., Dennis, B. R., Gabriel, A. H., and Simnett, G. M. 1985, *Solar Phys.*, **96**, 129.
Antonucci, E., Dodero, M. A., Gabriel, A. H., and Tanak, K. 1984a, in *Eighth International Colloquium on Ultraviolet and X-ray Spectroscopy of Astrophysical and Laboratory Plasmas, IAU Coll. No. 86* (Naval Research Laboratory, Washington, D. C.), p. 13.
Antonucci, E., Gabriel, A. H., Acton, L. W., Culhane, J. L., Doyle, J. G., Leibacher, J. W., Machado, M. E., Orwig, L. E., and Rapley, C. G. 1982, *Solar Phys.*, **78**, 107.
Antonucci, E., Gabriel, A. H., and Dennis, B. R. 1984b, *Astrophys. J.*, **287**, 917.
Antonucci, E., Rosner, R., and Tsinganos, K. 1986, *Astrophys. J.*, **301**, 975.
Bai, T., and Dennis, B. 1985, *Astrophys. J.*, **292**, 699.
Bentley, R. D., Lemen, J. R., Phillips, K. J. H., and Culhane, J. L. 1986, *Astron. Astrophys.* **154**, 255.
Canfield, R. C., and Gunkler, T. A. 1985, *Astrophys. J.*, **288**, 353.
Canfield, R. C., Metcalf, T. R., Strong, K. T., and Zarro, D. M. 1987, *Nature*, **326**, 165.
Cheng, C. C., Karpen, J. T., and Doschek, G. A. 1984, *Astrophys. J.*, **286**, 787.
Cheng, C. C., Tandberg-Hanssen, E., Bruner, E. C., Orwig, L., Frost, K. J., Kenny, P. J., Woodgate, B. E., and Shine, R. A. 1981, *Astrophys. J. Letters*, **248**, L39.
Cliver, E. W., Dennis, B. R,, Kiplinger, A. L., Kane, S. R., Neidig, D. F., Sheeley, N. R., Jr., and Koomen, M. J. 1986, *Astrophys. J.*, **305**, 920.
Culhane, J. L., Gabriel, A. H., Acton, L. W., Rapley, C. G., Phillips, K. J. H., Wolfson, C. J., Antonucci, E., Bentley, R. D., Catura, R. C., Jordan, C., Kayat, M. A., Kent, B. J., Leibacher, J. W., Parmar, A. N., Sherman, J. C., Springer, L. A., Strong, K. T., and Veck, N. J. 1981, *Astrophys. J. Letters*, **244**, L141.
de Jager, C. 1979, *Solar Phys.*, **64**, 135.
de Jager, C., and Švestka, Z. 1985, *Solar Phys.*, **100**, 435.
Dennis, B. R. 1985, *Solar Phys.*, **100**, 465.
Dere, K. P., Mason, H. E., Widing, K. G., and Bhatia, A. K. 1979, *Astrophys. J. Suppl.*, **40**, 341.
Doschek, G. A., Feldman, U., Kreplin, R. W., and Cohen, L. 1980, *Astrophys. J.*, **239**, 725.
Doschek, G. A., Feldman, U., Landecker, P. B., McKenzie, D. L. 1981, *Astrophys. J.*, **249**, 372.
Doschek, G. A., Kreplin, R. W., and Feldman, U. 1979, *Astrophys. J. Letters*, **233**, L157.
Doschek, G. A., and Tanaka, K. 1987, submitted to *Astrophys. J.*
Doyle, J. G., and Bentley, R. D. 1986, *Astron. Astrophys.*, **155**, 278.
Dubau, J., Gabriel, A. H., Loulergue, M., Steenman-Clark, L., and Volonté, S. 1981, *Monthly Notices Roy. Astron. Soc.*, **195**, 705.
Duijveman, A. 1983, *Solar Phys.*, **84**, 189.
Duijveman, A., and Hoyng, P. 1983, *Solar Phys.*, **86**, 279.
Emslie, A. G. 1981, *Astrophys. J.*, **245**, 711.
Feldman, U., Cheng, C.-C., and Doschek, G. A. 1982a, *Astrophys. J.*, **255**, 320.
Feldman, U., Doschek, G. A., and Kreplin, R. W. 1980a, *Astrophys. J.*, **238**, 365.
Feldman, U., Doschek, G. A., and Kreplin, R. W. 1982b, *Astrophys. J.*, **260**, 885.
Feldman, U., Doschek, G. A., Kreplin, R. W., and Mariska, J. T. 1980b, *Astrophys. J.*, **241**, 1175.
Fisher, G. H., Canfield, R. C., and McClymont, A. N. 1984, *Astrophys. J. Letters*, **281**, L79.
Haug, E. 1979, *Solar Phys.*, **61**, 129.
Hiei, E. 1982, *Solar Phys.*, **80**, 113.
Hiei, E., and Widing, K. G. 1979, *Solar Phys.*, **61**, 407.
Hirayama, T. 1974, *Solar Phys.*, **34**, 323.
Hoyng, P., Duijveman, A., Machado, M. E., Rust, D. M., Svestka, Z., Boelee, A., de Jager, C., Frost, K. J., LaFleur, H., Simnett, G. M., van Beek, H. F., and Woodgate, B. E. 1981, *Astrophys. J. Letters*, **246**, L155.
Inoue, H., Koyama, K., Mae, T., Matsuoka, M., Ohashi, T., Tanaka, Y., and Waki, I. 1982, *Nuclear Instr. Method*, **196**, 69.
Jacobs, V. L., Davis, J., Kepple, P. C., and Blaha, M. 1977, *Astrophys. J.*, **211**, 605.

Jordan, C. 1970, *Monthly Notices Roy. Astron. Soc.*, **148**, 17.
Kahler, S. W., and Kreplin, R. W. 1971, *Astrophys. J.*, **168**, 531.
Kai, K., Kosugi, T., and Nitta, N. 1985, *Publ. Astron. Soc. Japan*, **37**, 155.
Kane, S. R., Anderson, K. A., Evans, W. D., Klebesadel, R. W., and Laros, J. 1979, *Astrophys. J. Letters*, **233**, L151.
Kane, S. R., Chupp, E. L., Forrest, D. J., Share, G. H., and Rieger, E. 1986, *Astrophys. J. Letters*, **300**, L95.
Kawabata, K., Ogawa, H., and Suzuki, I. 1983, *Solar Phys.*, **86**, 247.
Kiplinger, A. L., Dennis, B. R., Emslie, A. G., Frost, K. J., and Orwig, L. E. 1983, *Astrophys. J. Letters*, **265**, L99.
Kondo, I. 1982, in *Hinotori Symposium on Solar Flares* (Institute of Space and Astronautical Science, Tokyo), p. 3.
Kopp, R. A., and Pneuman, G. W. 1976, *Solar Phys.*, **50**, 85.
Kosugi, T., and Tsuneta, S. 1983, *Solar Phys.*, **86**, 333.
Krutov, V. V., Korneev, V. V., Mandelstam, S. L., Sklyaptseva, A. S., Urnov, A. M., Vinogradov, A. V. 1981, *Lebedev Physical Institute Preprint*, No. 133.
Kundu, M., and Woodgate, B. (ed.) 1986, *Energetic Phenomena on the Sun*, NASA CP-2439 (National Technical Information Service, Springfield, Virginia).
Kurokawa, H. 1986, in *The Lower Atmosphere of Solar Flares*, ed. D. F. Neidig (National Solar Observatory/Sacramento Peak, Sunspot), p. 51.
Kurokawa, H., Kitahara, T., Nakai, Y., Funakoshi, Y., and Ichimoto, K. 1986, *Astrophys. Space Sci.*, **118**, 149.
Lin, R. P., Schwartz, R. A., Pelling, R. M., and Hurley, K. C. 1981, *Astrophys. J. Letters*, **251**, L109.
Machado, M. E., Duijveman, A., and Dennis, B. R. 1982, *Solar Phys.*, **79**, 85.
MacKinnon, A. L., Brown, J. C., and Hayward, J. 1985, *Solar Phys.*, **99**, 231.
Makishima, K. 1982, in *Hinotori Symposium on Solar Flares* (Institute of Space and Astronautical Science, Tokyo), p. 120.
Melrose, D. B., and Dulk, G. A. 1984, *Astrophys. J.*, **282**, 308.
Moore, R., McKenzie, D. L., Švestka, Z., Widing, K. G., Antiochos, S. K., Dere, K. P., Dodson-Prince, H. W,, Hiei, E., Krall, K. R., Krieger, A. S., Mason, H. E., Petrasso, R. D., Pneuman, G. W., Silk, J. K., Vorpahl, J. A., and Withbroe, G. L. 1980, in *Solar Flares*, ed. P. A. Sturrock, (Colorado Associated University Press, Boulder), p. 341.
Moriyama, F., Tanaka, K., Akita, K., Watanabe, T., Miyazaki, H., Miyashita, M., Kumagai, K., and Nishi, K. 1984, *Ann. Tokyo Astron. Obs.*, **19**, 276.
Nagai, F. 1980, *Solar Phys.*, **68**, 351.
Nakajima, H., Kosugi, T., Kai, K., and Enome, S. 1983, *Nature*, **305**, 292.
Neupert, W. M. 1968, *Astrophys. J. Letters*, **153**, L59.
Nishi, K., and Tanaka, K. 1984, in *Eighth International Colloquium on Ultraviolet and X-ray Spectroscopy of Astrophysical and Laboratory Plasmas, IAU Coll. No. 86* (Naval Research Laboratory, Washington, D. C.), p. 1.
Nitta, N., Takakura, T., Ohki, K., and Yoshimori, M. 1983, *Solar Phys.*, **86**, 241.
Oda, M. 1965, *Appl. Optics*, **4**, 143.
Ohki, K., Takakura, T., Tsuneta, S., and Nitta, N. 1983, *Solar Phys.*, **86**, 301.
Pallavicini, R., Serio, S., and Vaiana, G. S. 1977, *Astrophys. J.*, **216**, 108.
Parmar, A. N., Culhane, J. L., Rapley, C. G., Antonucci, E., Gabriel, A. H., and Loulergue, M. 1981, *Monthly Notices Roy. Astron. Soc.*, **197**, 29P.
Parmar, A. N., Wolfson, C. J., Culhane, J. L., Phillips, K. J. H., Acton, L. W., Dennis, B. R., and Rapley, C. G. 1984, *Astrophys. J.*, **279**, 866.
Phillips, K. J. H., and Neupert, W. M. 1973, *Solar Phys.*, **32**, 209.
Rieger, E., Reppin, C., Kanbach, G., Forrest, D. J., Chupp, E. L., and Share, G. H. 1983, *Procedings of 18th International Cosmic Ray Conference, Vol. 4*, ed. N. Durgaprasad, S. Ramadurai, P. V. Ramana Murthy, M. V. S. Rao, and K. Sivaprasad (Tata Institute of Fundamental Research, Bombay), p. 83.
Rosner, R., Tucker, W. H., and Vaiana, G. S. 1978, *Astrophys. J.*, **220**, 643.

Roy, J.-R., and Tang, F. 1975, *Solar Phys.*, **42**, 425.
Sakurai, T. 1983, *Solar Phys.*, **86**, 339.
Sakurai, T. 1985, *Solar Phys.*, **95**, 311.
Seely, J. F., and Feldman, U. 1984, *Astrophys. J. Letters*, **280**, L59.
Shlyaptseva, A. S., Urnov, A. M., and Vinogradov, A. V. 1981, *Lebedev Physical Institute Preprint*, No. 193.
Shull, J. M., and Van Steenberg, M. 1982, *Astrophys. J. Suppl.*, **48**, 95.
Smith, D. F., and Auer, L. H. 1980, *Astrophys. J.*, **238**, 1126.
Sugihara, R., and Midzno, Y. 1979, *J. Phys. Soc. Japan*, **47**, 1290.
Tajima, T., Brunel, F., and Sakai, J. 1982, *Astrophys. J. Letters*, **258**, L45.
Takakura, T. 1984, *Solar Phys.*, **91**, 311.
Takakura, T. 1985, in *Proceedings of International Workshop on Solar Physics and Interplanetary Travelling Phenomena, Kunming 1983*, ed. C. de Jager and Chen Biao (Science Press, Beijing), p. 427.
Takakura, T. 1986, *Solar Phys.*, **104**, 363.
Takakura, T., Kaufmann, P., Costa, J. E. R., Degaonkar, S. S., Ohki, K., and Nitta, N. 1983a, *Nature*, **302**, 317.
Takakura, T., Ohki, K., Nitta, N., and Wang, J. L. 1984a, *Astrophys. J. Letters*, **281**, L51.
Takakura, T., Ohki, K., Sakurai, T., Wang, J. L., Xuan, J. Y., Li, S. C., and Zhao, R. Y. 1984b, *Solar Phys.*, **94**, 359.
Takakura, T., Ohki, K., Tsuneta, S,, and Nitta, N. 1983b, *Solar Phys.*, **86**, 323.
Takakura, T., Tanaka, K., and Hiei, E. 1984c, *Adv. Space Res.*, **4**, No. 7, 143 (TTH84).
Takakura, T., Tanaka, K., Nitta, N., Kai, K., and Ohki, K. 1987, *Solar Phys.*, **107**, 109.
Takakura, T., Tsuneta, S., Ohki, K,, Nitta, N., Makishima, K., Murakami, T., Ogawara, Y., Oda, M., and Miyamoto, S. 1983c, *Astrophys. J. Letters*, **270**, L83.
Tanaka, K. 1976, *Solar Phys.*, **47**, 247.
Tanaka, K. 1978, *Solar Phys.*, **58**, 149.
Tanaka, K. 1980, in *Proceedings of the Japan-France Seminar on Solar Physics*, ed. F. Moriyama and J. C. Henoux (Tokyo Astronomical Observatory, Tokyo), p. 219.
Tanaka, K. 1983, *Activity in Red-Dwarf Stars, IAU Coll. 71*, ed. P. B. Byrne and M. Rodonō (Reidel, Dordrecht), p. 307.
Tanaka, K. 1986a, *Astrophys. Space Sci.*, **118**, 101.
Tanaka, K. 1986b, *Publ. Astron. Soc. Japan*, **38**, 225.
Tanaka, K. 1986c, in *Hydrodynamic and Magnetohydrodynamic Problems in the Sun and Stars*, ed. Y. Osaki (Department of Astronomy, University of Tokyo, Tokyo), p. 1.
Tanaka, K., Akita, K., Watanabe, T., Miyazaki, H., Kumagai, K., Miyashita, M., Nishi, K., and Moriyama, F. 1982a, *Ann. Tokyo Astron. Obs.*, **18**, 237.
Tanaka, K., Akita, K., Watanabe, T., and Nishi, K. 1982b, in *Hinotori Symposium on Solar Flares* (Institute of Space and Astronautical Science, Tokyo), p. 43.
Tanaka, K., and Nakagawa, Y. 1973, *Solar Phys.*, **33**, 187.
Tanaka, K., and Nishi, K. 1978, *Japanese J. Appl. Phys. Suppl.*, **17**, 461.
Tanaka, K., Nitta, N., Akita, K., and Watanabe, T. 1983, *Solar Phys.*, **86**, 91.
Tanaka, K., Nitta, N., and Watanabe, T. 1982c, in *Hinotori Symposium on Solar Flares* (Institute of Space and Astronautical Science, Tokyo), p. 20.
Tanaka, K., Smith, Z., and Dryer, M. 1980, in *Solar and Interplanetary Dynamics, IAU Symp. No. 91*, ed. M. Dryer and E. Tandberg-Hanssen (Reidel, Dordrecht), p. 231.
Tanaka, K., Watanabe, T., Nishi, K., and Akita, K. 1982d, *Astrophys. J. Letters*, **254**, L59.
Tanaka, K., Watanabe, T., Nitta, N. 1984, *Astrophys. J.*, **282**, 793.
Tanaka, K., and Zirin, H. 1985, *Astrophys. J.*, **299**, 1036 (TZ85).
Tanaka, Y. 1983, *Solar Phys.*, **86**, 3.
Tramiel, L. J., Chanan, G. A., and Novick, R. 1984, *Astrophys. J.*, **280**, 440.
Tsuneta, S. 1984a, *Ann. Tokyo Astron. Obs.*, **20**, 1.
Tsuneta, S. 1984b, in *Active Phenomena in the Outer Atmosphere of the Sun and Stars*, ed. J.-C. Pecker and Y. Uchida (Observatoire de Paris, Meudon), p. 243.

Tsuneta, S. 1985, *Astrophys. J.*, **290**, 353.
Tsuneta, S., Nitta, N., Ohki, K., Takakura, T., Tanaka, K., Makishima, K., Murakami, T., Oda, M., and Ogawara, Y. 1984a, *Astrophys. J.*, **284**, 827.
Tsuneta, S., Takakura, T., Nitta, N., Ohki, K., Makishima, K., Murakami, T., Oda, M., and Ogawara, Y. 1983, *Solar Phys.*, **86**, 313.
Tsuneta, S., Takakura, T., Nitta, N., Ohki, K., Tanaka, K., Makishima, K., Murakami, T., Oda, M., Ogawara, Y., and Kondo, I. 1984b, *Astrophys. J.*, **280**, 887.
Uchida, Y., and Shibata, K. 1984, in *Unstable Current Systems and Plasma Instabilities in Astrophysics*, *IAU Symp. No. 105*, ed. M. Kundu and G. Holman (Reidel, Dordrecht), p. 287.
Vorpahl, J. A. 1972, *Solar Phys.*, **26**, 397.
Watanabe, T. 1984a, in *Active Phenomena in the Outer Atmosphere of the Sun and Stars*, ed. J.-C. Pecker and Y. Uchida (Observaoire de Paris, Meudon), p. 230.
Watanabe, T. 1984b, in *Active Phenomena in the Outer Atmosphere of the Sun and Stars*, ed. J. C. Pecker and Y. Uchida (Observatorie de Paris, Meudon), p. 289.
Watanabe, T., Tanaka, K., Akita, K., and Nitta, N. 1983, *Solar Phys.*, **86**, 107.
Watanabe, T., Tanaka, K., and Matsuoka, M. 1982, in *Hinotori Symposium on Solar Flares* (Institute of Space and Astronautical Science, Tokyo), p. 14.
Widing, K. G., and Dere, K. P. 1977, *Solar Phys.*, **55**, 431.
Yoshimori, M. 1985, *J. Phys. Soc. Japan*, **54**, 487.
Yoshimori, M., Okudaira, K., and Yanagimachi, T. 1986, *J. Phys. Soc. Japan*, **55**, 3683.
Yoshimori, M., Watanabe, H., and Nitta, N. 1985, *J. Phys. Soc. Japan*, **54**, 4462.
Zirin, H., and Tanaka, K. 1973, *Solar Phys.*, **32**, 173.